2016

IMPROVED CAPABILITY OF A COMPUTATIONAL FOOT/ANKLE MODEL USING ARTIFICIAL NEURAL NETWORKS

Ruchi D. Chande
Virginia Commonwealth University

IMPROVED CAPABILITY OF A COMPUTATIONAL FOOT/ANKLE MODEL

USING ARTIFICIAL NEURAL NETWORKS

A Dissertation submitted in partial fulfillment of the requirements for the degree of Doctor of Philosophy at Virginia Commonwealth University.

by

RUCHI DILIP CHANDE
Master of Science, Virginia Commonwealth University, 2012
Bachelor of Science, University of California, Berkeley, 2006

Director: Dr. Jennifer S. Wayne
Professor, Departments of Biomedical Engineering & Orthopaedic Surgery
Director, Orthopaedic Research Laboratory

Virginia Commonwealth University
Richmond, Virginia
May 2016

Acknowledgements

Wow…I can't believe I finally made it here. My journey over the past four and a half years has truly tried and tested me in the deepest of ways, but I am proud to say I made it to the other side—and I am still standing. Through all the highs and lows, many people were there for me and I must give thanks.

First, to my advisor Dr. Jennifer Wayne, I give thanks for guiding me through my graduate career. You have afforded me many opportunities, not only in research, but in teaching and leadership, all of which helped me explore my interests. Throughout it all, I learned a great deal about myself, and as a result, gained more self-confidence. I can honestly say that I will leave ORL and VCU with a sense of accomplishment and renewed excitement for the future.

To the faculty who so kindly served on my committee—Dr. Gerald Miller, Dr. Norma Ortiz-Robinson, Dr. Paul Wetzel, and Dr. Rosalyn Hargraves—I want to convey my sincerest appreciation for your willingness to answer my many questions, but mostly for believing in and encouraging me. Such kind words are not and will not be lost on me.

To my friends from lab, past and present, your company has eased the long journey. Johnny, Meade, Alex, EJ, Nathan, and Brandon, your friendship, humor, and company in the lab were much appreciated. Beyond lab, I have to thank Amritha, Trish, Nadiah, Lauren, Gigi, Afsar, Allen, Peggy, Mona, Magda, and Wendy—you all offered support, encouragement, and friendship, always.

To Justin Osborne, I cannot thank you enough for access to my very own fleet of computers! To Dr. Vojislav Kecman, your willingness to invest time in me and share your knowledge was so meaningful to me—thank you! To Laura Lemza, you went above and beyond to help me. You have always taken the time to listen, answer questions, and give good advice that was applicable well beyond career. Your kindness will always stick with me—thank you for being a friend. To Tori Keel, I cannot begin to fully express the amount of gratitude I have for you. You listened, you never judged, you advised, you reassured, all while letting me figure things out. I learned a lot about myself, and with your invaluable help, I made it to the end! Please know that you made an incredible impact on me and that I will always be grateful. Thank you.

And last but not least, I must thank my family. To my parents, Dilip and Pallavi Chande, you have always been great cheerleaders. You always believed I could and would be amazing and you never let me think anything less. You never missed an opportunity to tell me how proud you were of me. Dad would say "we are Chandes" and mom would say "you're our kid!" You always reassured me that success was never a question—it was a given. For this, among many reasons, I am thankful for you both and I love you both so much. Neha! We just get each other! You are my voice of reason! I look up to you and admire you so much. You are intelligent, beautiful, thoughtful, funny, humble, and just an all-around amazing sister. Ever since I was little, you would always give me a hug, comfort me, and remind me who I was—you just made it all better. You still make it all better. You are absolutely the best—don't forget it. I love you.

Looking back, all I can say is that mine is a life truly blessed with good people.

Table of Contents

Page

Acknowledgements ii

List of Tables vi

List of Figures vii

Chapter

1 Introduction 1

1.1 Significance of Computational Modeling 1

1.2 Using Computational Modeling to Study Adult-Acquired Flatfoot Deformity 2

1.2.1 Foot and Ankle Anatomy 2

1.2.2 Adult-Acquired Flatfoot Deformity 9

1.2.3 Patient-Specific Computational Foot/Ankle Models of AAFD 10

1.3 Informing the Structure - Function Relationship 13

1.4 Artificial Neural Networks 14

1.4.1 General Neural Network Structure 15

1.4.2 Learning Rules 17

1.4.3 Training Methods 18

1.4.4 General Uses and Applications to Biomedical and Biomechanical Models 21

1.4.5 Preliminary Neural Network Study 23

1.5 Objective 23

2 Methods 25
2.1 Predictions for Pre-Operative Foot/Ankle Model 25
2.2 Predictions for Post-Operative Foot/Ankle Model 36
2.3 Effect of Stiffness Variation on Angular Measures 36
3 Results 38
3.1 Pre-operative Results 38
3.2 Post-operative Results 43
3.3 Effect of Ligament Group on Kinematics, Pre-operative Data 46
3.4 Effect of Ligament Group on Kinematics, Post-operative Data 55
4 Discussion 62
4.1 Artificial Neural Network Usage 62
4.2 Us of Single Patient Foot/Ankle Model for Data Generation 64
4.3 Kinematic Ranges, Pre- and Post-Operative 65
4.4 Neural Network Performance, Pre- and Post-Operative 66
4.5 Training Methodologies; Network Sizes 67
4.6 Ligament Stiffness Predictions 70
4.6.1 ANN-Predicted Stiffnesses versus Assigned Foot/Ankle Model Stiffnesses 70
4.6.2 Link between Insignificant Trends and ANN-Predicted Stiffnesses . 72
4.6.3 ANN-Predicted Stiffnesses for Patient Radiographic Data 72
4.7 Foot/Ankle Model Performance using ANN-Predicted Stiffnesses 75
4.8 Relationship between Kinematic Measures and Ligament Groupings . 80

4.9 Overall Discussion and Future Directions 85

Literature Cited 88

Appendices 91

Vita 95

List of Tables

Page

Table 2.1: Starting Values, Ligament Stiffnesses. 28

Table 3.1: Optimal Network Performance, Pre-operative Data. 39

Table 3.2: Parameters Corresponding to Optimal Networks, Pre-operative Data. 40

Table 3.3: Target Ligament Stiffnesses (Pre-Op) vs. ANN-Predicted Stiffnesses. 41

Table 3.4: Stiffness Predictions for Pre-Op X-Ray Kinematics. 42

Table 3.5: Pre-Operative Kinematic Measures. 42

Table 3.6: Percent Difference Relative to Pre-Op Radiograph. 42

Table 3.7: Optimal Network Performance, Post-operative Data. 44

Table 3.8: Parameters Corresponding to Optimal Networks, Post-operative Data..... 44

Table 3.9: Target Ligament Stiffnesses (Post-Op Model) vs. ANN-Predicted Stiffnesses .

..... 44

Table 3.10: Stiffness Predictions for Post-Op X-Ray Kinematics. 45

Table 3.11: Post-Operative Kinematic Measures..... 45

Table 3.12: Percent Difference Relative to Post-Op Patient Radiograph. 46

Table 3.13: p-values, Talo-1st Metatarsal Angle versus Percent Stiffness Variation. 47

Table 3.14: p-values, Talo-Navicular Angle versus Percent Stiffness Variation. 50

Table 3.15: p-values, Talo-1st Metatarsal Angle versus Percent Stiffness Variation. 54

Table 3.16: p-values, Talo-Navicular Angle versus Percent Stiffness Variation. 58

List of Figures

Page

Figure 1.1: Ankle Joint 3

Figure 1.2: Bony Foot 4

Figure 1.3: Medial Longitudinal Arch 5

Figure 1.4: Deltoid Ligament 6

Figure 1.5: Spring Ligament, Plantar fascia, Talocalcaneal Interosseous Ligament. 7

Figure 1.6: Musculature 8

Figure 1.7: Pre-operative, Patient-Specific Model 11

Figure 1.8: Bony Anatomy with Surgical Correction, Post-operative, Patient Specific Model 12

Figure 1.9: Neuron schematics 16

Figure 1.10: Network architectures 17

Figure 1.11: Cross-validation 20

Figure 2.1: Task Flow 26

Figure 2.2: Kinematic Measures 27

Figure 2.3: Feedforward Network 30

Figure 2.4: Random Number Generator 32

Figure 2.5: Radial Basis Function Network 35

Figure 3.1: Pre-operative Angular Data. 38

Figure 3.2: Post-operative Angular Data. 43

Figure 3.3: Talo-1st Metatarsal Angle, Medial Variation, from normal (pre-op). 47

Figure 3.4: Talo-1st Metatarsal Angle, Medial Variation, from attenuation (pre-op). 48

Figure 3.5: Talo-1st Metatarsal Angle, Plantar Variation, from normal (pre-op). 48

Figure 3.6: Talo-1st Metatarsal Angle, Plantar Variation, from attenuation (pre-op). 49

Figure 3.7: Talo-1st Metatarsal Angle, Spring Variation, from normal (pre-op). 49

Figure 3.8: Talo-1st Metatarsal Angle, Spring Variation, from attenuation (pre-op)..... 50

Figure 3.9: Talo-Navicular Angle, Medial Variation, from normal (pre-op). 51

Figure 3.10: Talo-Navicular Angle, Medial Variation, from attenuation (pre-op)..... 51

Figure 3.11: Talo-Navicular Angle, Plantar Variation, from normal (pre-op). 52

Figure 3.12: Talo-Navicular Angle, Plantar Variation, from attenuation (pre-op)..... 52

Figure 3.13: Talo-Navicular Angle, Spring Variation, from normal (pre-op). 53

Figure 3.14: Talo-Navicular Angle, Spring Variation, from attenuation (pre-op)..... 53

Figure 3.15: Talo-1st Metatarsal Angle, Medial Variation, from normal (post-op)..... 55

Figure 3.16: Talo-1st Metatarsal Angle, Medial Variation, from attenuation (post-op). .. 55

Figure 3.17: Talo-1st Metatarsal Angle, Plantar Variation, from normal (post-op)..... 56

Figure 3.18: Talo-1st Metatarsal Angle, Plantar Variation, from attenuation (post-op). .. 56

Figure 3.19: Talo-1st Metatarsal Angle, Spring Variation, from normal (post-op)..... 57

Figure 3.20: Talo-1st Metatarsal Angle, Spring Variation, from attenuation (post-op). ... 57

Figure 3.21: Talo-Navicular Angle, Medial Variation, from normal (post-op)..... 58

Figure 3.22: Talo-Navicular Angle, Medial Variation, from attenuation (post-op). 59

Figure 3.23: Talo-Navicular Angle, Plantar Variation, from normal (post-op)..... 59

Figure 3.24: Talo-Navicular Angle, Plantar Variation, from attenuation (post-op). 60

Figure 3.25: Talo-Navicular Angle, Spring Variation, from normal (post-op). 60

Figure 3.26: Talo-Navicular Angle, Spring Variation, from attenuation (post-op). 61

Figure 4.1: Ligamentous Support of Medial Longitudinal Arch. 77

Figure 4.2: Talo-Navicular Angle 79

Abstract

IMPROVED CAPABILITY OF A COMPUTATIONAL FOOT/ANKLE MODEL USING ARTIFICIAL NEURAL NETWORKS

By Ruchi Dilip Chande, M.S.

A Dissertation submitted in partial fulfillment of the requirements for the degree of Doctor of Philosophy in Biomedical Engineering at Virginia Commonwealth University.

Virginia Commonwealth University, 2016.

Major Director: Jennifer S. Wayne, Ph.D.
Professor, Departments of Biomedical Engineering & Orthopaedic Surgery
Director, Orthopaedic Research Laboratory

Computational joint models provide insight into the biomechanical function of human joints. Through both deformable and rigid body modeling, the structure-function relationship governing joint behavior is better understood, and subsequently, knowledge regarding normal, diseased, and/or injured function is garnered. Given the utility of these computational models, it is imperative to supply them with appropriate inputs such that model function is representative of true joint function. In these models, Magnetic Resonance Imaging (MRI) or Computerized Tomography (CT) scans and literature inform

the bony anatomy and mechanical properties of muscle and ligamentous tissues, respectively. In the case of the latter, literature reports a wide range of values or average values with large standard deviations due to the inability to measure the mechanical properties of soft tissues *in vivo*. This makes it difficult to determine which values within the published literature to assign to computational models, especially patient-specific models. Therefore, while the use of published literature serves as a reasonable first approach to set up a computational model, a means of improving the supplied input data was sought.

This work details the application of artificial neural networks (ANNs), specifically feedforward and radial basis function networks, to the optimization of ligament stiffnesses for the improved performance of pre- and post-operative, patient-specific foot/ankle computational models. ANNs are mathematical models that utilize learning rules to determine relationships between known sets of inputs and outputs. Using knowledge gained from these training data, the ANN may then predict outputs for similar, never-before-seen inputs. Here, an optimal network of each ANN type was found, per mean square error and correlation data, and then both networks were used to predict optimal ligament stiffnesses corresponding to a single patient's radiographic measurements. Both sets of predictions were ultimately supplied to the patient-specific computational models, and the resulting kinematics illustrated an improvement over the existing models that utilized literature-assigned stiffnesses. This research demonstrated that neural networks are a viable means to hone in on ligament stiffnesses for the overall objective of improving the predictive ability of a patient-specific computational model.

CHAPTER 1 Introduction

1.1 Significance of Computational Modeling

Computational modeling of human joints has been employed to study both joint kinematics and deformation, and simultaneously gain insight into how joint structure affects its function. More specifically, studies using these computational models have explored topics including, but not limited to, the motion of joints and the relative positions of one bone to another following load simulation, as well as the forces or stresses acting on joints due to everyday activities, injury, or the placement of corrective hardware [1-10]. Such models are beneficial in that simulations can run relatively quickly, a variety of testing conditions can be investigated, and test conditions may be repeated multiple times if needed. As a result, computational modeling sheds light on normal joint function and also allows for the characterization and comparison of diseased and injured states. Information garnered from these comparisons may then elucidate treatment options for joint ailments or design developments for devices used in corrective procedures. Given their utility, it is imperative to supply computational models with the proper inputs as these directly affect the strength of the models' predictions.

1.2 Using Computational Modeling to Study Adult-Acquired Flatfoot Deformity

Biomechanics of the wrist, shoulder, and elbow, as well as the foot/ankle complex have all been studied using computational modeling [1-2, 4, 8-10]. Such investigations have included kinematic studies, as well as finite element analyses revealing stress or strain due to hardware fixation. Within the Orthopaedic Research Laboratory (ORL) at Virginia Commonwealth University (VCU), the foot/ankle complex, in particular, has been a primary focus in the study of Adult-Acquired Flatfoot Deformity (AAFD). In previous work, the ORL (in collaboration with the Department of Orthopaedic Surgery at VCU) developed multiple patient-specific foot/ankle models to investigate the effects on foot kinematics of the pre-operative AAFD state, as well as the post-operative state following implementation of a surgical correction [2, 11].

1.2.1 Foot and Ankle Anatomy

In order to understand AAFD, its effects, and thus the scope of those models developed by the ORL, foot and ankle anatomy must first be explored. Here, an anatomical overview will be provided with emphasis on those bony and soft tissues that are most pertinent to the current study. The foot and ankle are comprised of twenty eight bones surrounded and supported by many ligamentous tissues and musculature. Beginning with the bony anatomy and most proximal joint, the ankle (tibiotalar) joint (Figure 1.1) is defined as the articulation between the tibia and the talus; the former being the larger of the two bones of the lower leg. Specifically, the distally located tibial plafond, which has a generally flat shape and is approximately perpendicular to the tibial shaft axis, articulates with the talar dome, while the further distally located medial malleolus of the tibia

articulates with the medial surface of the talus [12, 13]. Similarly, a distally located projection known as the lateral malleolus on the fibula, the lateral bone of the lower leg, articulates with the lateral surface of the talus. Due to the arched shape created by the tibial and fibular surfaces above and around the talar dome, the ankle joint is often described as a mortise [13] and serves to simultaneously support weight-bearing activities while keeping extreme movements in check [14-15].

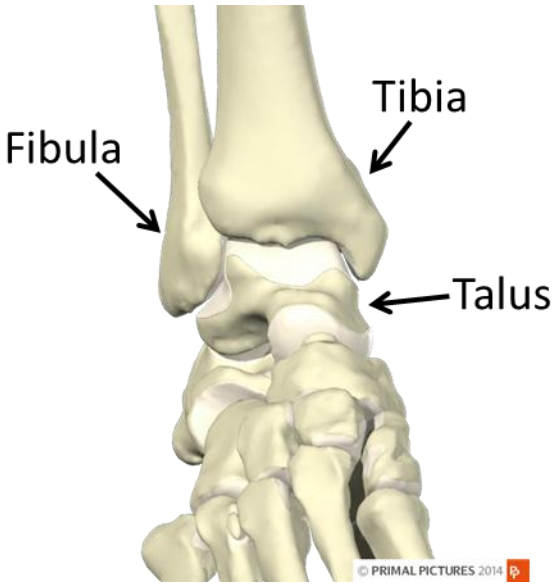

Figure 1.1: Ankle Joint (right), anterior view. The articular surfaces of the tibia and fibula meet with those of the talus to create the mortise shape of the ankle joint. [Adapted from: Primal Pictures for Anatomy TV.]

Just inferior to the talus is the calcaneus, and these bones together define the hindfoot division of the foot [16] (Figure 1.2). The inferior surface of the talus articulates with the middle, anterior, and posterior articulating surfaces on the superior calcaneus [16] and is further supported medially by a wing-shaped bony protrusion called the sustentaculum tali [17]. Anterior to the hindfoot is the midfoot, which is comprised of the navicular, 1st cuneiform, 2nd cuneiform, 3rd cuneiform (synonymously known as the medial, intermediate, and lateral cuneiforms, respectively), and cuboid [16]. The navicular

bone, which is named as such due to its boat-like shape [16], is located medially and shares articulations with both the talar head posteriorly and the 1st through 3rd cuneiforms anteriorly [13, 16]. Finally, anterior to the midfoot is the forefoot which consists of the 1st through 5th metatarsal bones (named medial to lateral with the 1st metatarsal being the thickest of the five [16]) and fourteen phalanges making up the toes [16-17]. Of note, the proximal articular surface of the 1st metatarsal, which is known as the base, interfaces with the anterior articular surface of the 1st cuneiform of the midfoot, while medial and lateral sesamoid bones (Figure 1.3) lie just inferior to the plantar surface of the 1st metatarsal bone [13, 16-17].

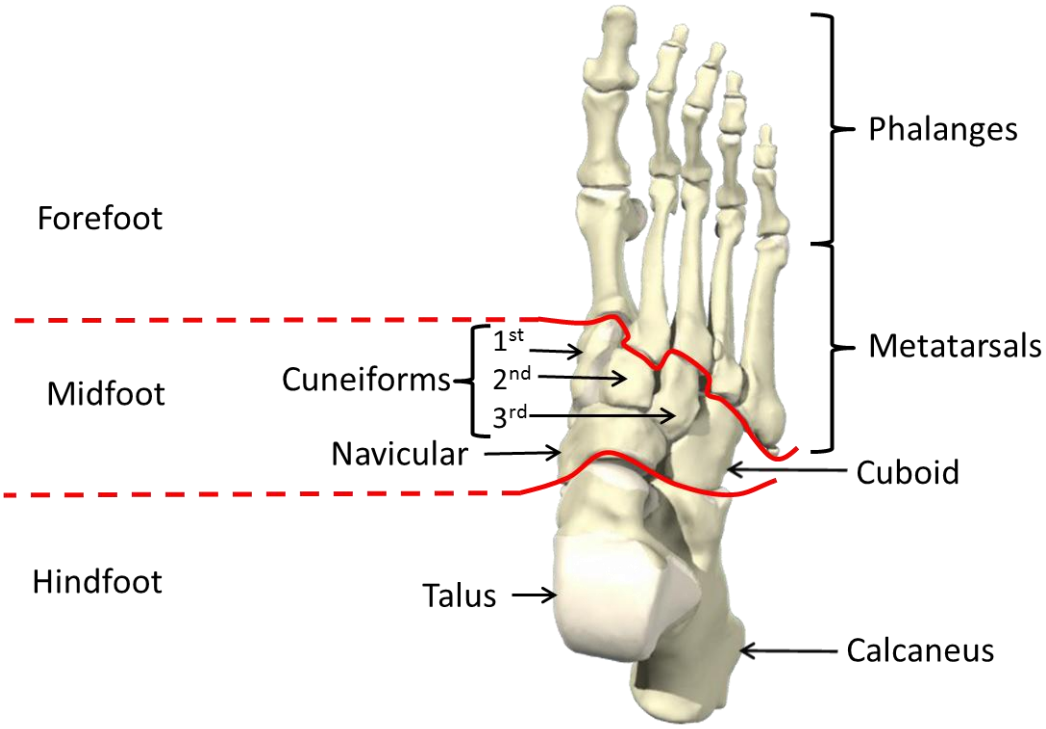

Figure 1.2: Bony Foot (right), dorsal view. The bones comprising the foot are shown, and the red lines depict the two boundaries that separate these bones into the three divisions of the foot: hindfoot, midfoot, and forefoot (from posterior to anterior). [Adapted from: Primal Pictures for Anatomy TV.]

Just as the foot is said to be divided into a hindfoot, midfoot, and forefoot when traveling posteriorly to anteriorly, it can also be divided into medial and lateral longitudinal arches in the sagittal plane (Figure 1.3). Of particular relevance to the current work is the medial longitudinal arch consisting of the calcaneus, talus, navicular, cuneiforms, and 1st through 3rd metatarsals. In a normal foot, this arch does not contact the ground when standing upright; thus a noticeable flattening of this arch indicates flatfoot and is a hallmark of AAFD [11, 16-17].

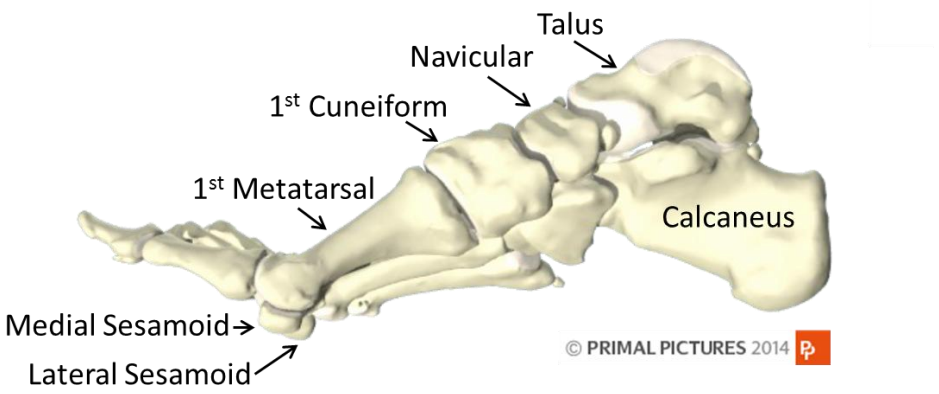

Figure 1.3: Medial Longitudinal Arch (right foot), medial view. Most of the bones belonging to the medial longitudinal arch are depicted here. Though not part of the arch, the medial and lateral sesamoid bones are also depicted as they are visible just inferior to the 1st metatarsal. [Adapted from: Primal Pictures for Anatomy TV.]

While several ligamentous structures reinforce the many joints of the foot and ankle, focus here will lie on those structures implicated in AAFD: the deltoid, spring, plantar, and talo-calcaneal interosseous ligaments. The ankle joint is spanned on its medial side by the deltoid ligament, a portion of tissue that actually consists of multiple parts (Figure 1.4). All originating on the medial malleolus, the anterior tibiotalar, tibionavicular, tibiocalcaneal, and posterior tibiotalar ligaments travel distally and fan out to insert onto the anterior talus, navicular, sustentaculum tali of the calcaneus, and posterior talus,

respectively [13, 17]. Additionally, the tibiospring ligament inserts onto yet another soft tissue of importance: the spring ligament complex [18-19]. Functionally, the deltoid ligaments serve to resist eversion of the ankle in which the plantar surface of the foot faces laterally outward [13, 17].

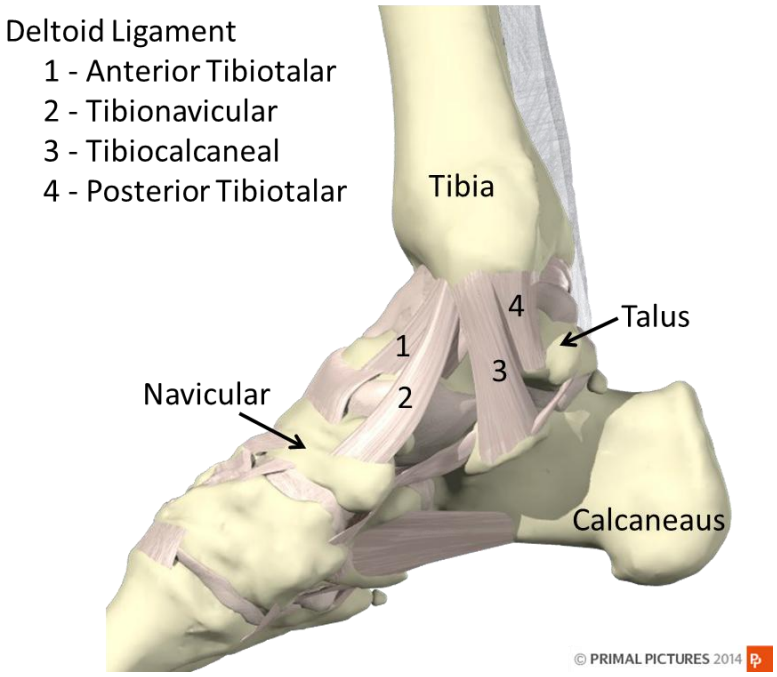

Figure 1.4: Deltoid Ligament (right ankle), medial view. The deltoid ligament is comprised of multiple bands that originate on the tibia and fan out to insert onto the talus, navicular, and calcaneus. [Adapted from: Primal Pictures for Anatomy TV.]

The spring ligament complex (Figure 1.5A) alluded to previously is more specifically known as the calcaneonavicular ligaments and has three distinct sections. The superomedial portion originates on the medial and anterior borders of the sustentaculum tali of the calcaneus and reaches out anteriorly and medially to wrap around the tuberosity and dorsomedial surface of the navicular [13, 17]. The medial calcaneonavicular band also begins on the calcaneus, just lateral to the superomedial portion, and attaches both medially and inferiorly on the navicular. Finally, the inferomedial band attaches inferiorly

on the calcaneus and inserts just lateral to the middle band on the inferior navicular [17]. Generally, this ligament complex is thought to support the talonavicular joint [16-17] and thus supports the medial arch of the foot [13].

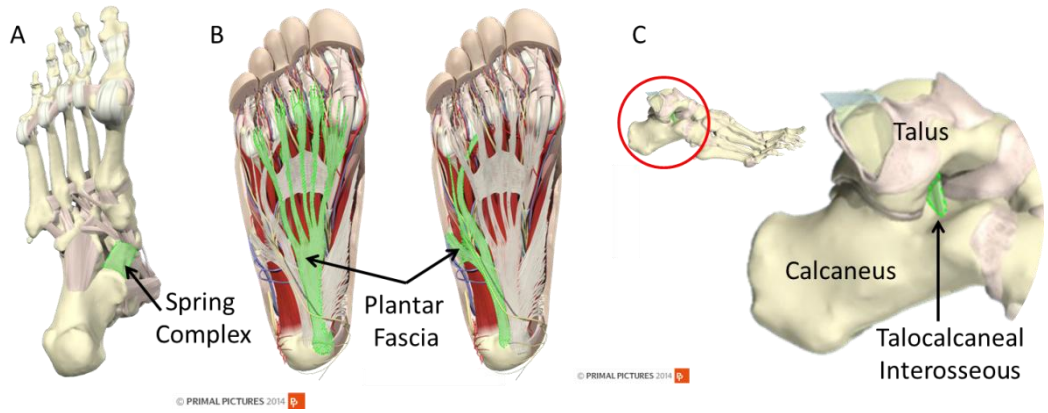

Figure 1.5: (A) Spring Ligament (right foot), inferomedial view. The entire complex is thought to play a role in supporting the talar head. (B) Plantar fascia (right foot), plantar view. Bands of the plantar fascia travel both anteriorly to the metatarsal heads, as well as anterolaterally to insert on the 5th metatarsal. (C) Talocalcaneal Interosseous Ligament (right ankle), lateral view. This ligament spans the articulation between the talus and calcaneus in the interior of the foot. [Adapted from: Primal Pictures for Anatomy TV.]

The plantar fascia bands span the plantar surface of the foot from the inferior-most surface of the calcaneus to the distally located metatarsal heads, as well as a smaller portion extending anteriorly and laterally to insert on the proximal end of the 5th metatarsal [11, 13, 17] (Figure 1.5B). The vast posterior to anterior reach of the plantar fascia aids in pulling the foot taut thereby emphasizing the medial arch of the foot [11, 17]. Finally, the talocalcaneal interosseous ligament provides support to the talocalcaneal joint by spanning a broad width of space between the two bones (Figure 1.5C). It travels an angled course to support the joint posteriorly and then melds with the joint capsule surrounding the talocalcaneonavicular joint anteriorly [13].

Regarding musculature supporting the foot and ankle, three muscles of the posterior compartment of the leg will be the focus due to their relationship with the medial longitudinal arch. The first of these is the Posterior Tibialis muscle, which is the deepest and centrally located (Figure 1.6A). This muscle originates on the interosseous membrane (a fibrous connection spanning the diaphyseal lengths of the tibia and fibula), the posteromedial surface of the fibula, and posterosuperior surface of the tibia and travels distally and medially, wrapping inferior to the medial malleolus of the tibia and subsequently entering the foot. The tendon of the Posterior Tibialis (PTT) passes just beneath the spring ligament and has its major insertion site on the navicular tuberosity. As this attachment exists on a bone belonging to the medial longitudinal arch, it becomes obvious that the Posterior Tibialis contributes to inversion of the foot [13].

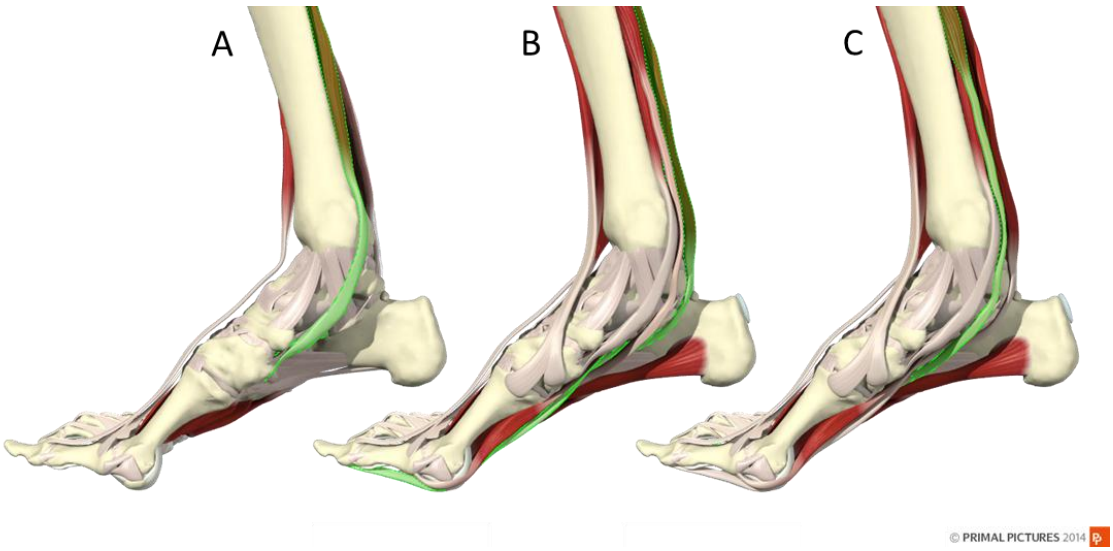

Figure 1.6: Musculature (right foot/ankle), medial view. (A) Posterior Tibialis; (B) Flexor Hallucis Longus; (C) Flexor Digitorum Longus. [Adapted from: Primal Pictures for Anatomy TV.]

Deep and medial to the Posterior Tibialis is the Flexor Hallucis Longus (FHL) (Figure 1.6B). This muscle also has origins on the interosseous membrane and the

posterior surface of the fibula. Its tendon travels distally and curves around the posterior surface of the talus and beneath the sustentaculum tali to finally insert on the inferior surface of the base of the distal phalanx of the great toe. Among other functions, the FHL acts to flex the great toe and provides an additional means to invert the foot [13].

The third muscle of significance here is the most medially arising muscle of the posterior leg compartment (Figure 1.6C). The Flexor Digitorum Longus (FDL) begins on the posterior tibia, courses distally and posteriorly to the medial malleolus, travels next to the sustentaculum tali of the calcaneus superficial to the tibiocalcaneal ligament, and finally enters the foot. Final insertions exist on the bases of the distal phalanges of toes 2-5 as the tendon of the FDL separates into four sections. This muscle's primary action is to flex the toes upon which it inserts [13].

1.2.2 Adult-Acquired Flatfoot Deformity

As mentioned earlier, the Posterior Tibialis muscle is a primary inverter of the foot, and so its deterioration can lead to gradual changes in the shape of the medial longitudinal arch. Specifically, the talar head shifts medially while the forefoot moves laterally, thus resulting in an opening of the talonavicular joint (commonly referred to as "uncoverage" of the talar head) [20-22]. The gross joint misalignment described here, and occurring secondarily to PTT dysfunction [23], is known as AAFD. While cause of PTT dysfunction is not fully understood, it subsequently leads to weakening of additional soft tissue constraints, specifically the spring, deltoid, plantar, and talo-calcaneal interosseous ligaments [23-27]. This tissue weakening results from increased loading placed on the tissues [13] following the PTT's inability to adequately support the talo-navicular joint

[25]. The deformity is most easily (grossly) identifiable as a fallen arch [13] and hindfoot valgus (medial tilting of the ankle), and results in pain for the patient upon ambulation [20, 24-25, 28-29]. Because the deformity can range in severity, many corrective procedures like tendon transfers and medializing calcaneal osteotomies (MCOs) [23, 30] exist to restore foot/ankle function by doing one or more of the following: replacing lost PTT function (candidates for PTT replacement include the FHL and FDL [20, 27, 31]), restoring the foot's arch, correcting hindfoot valgus [29-30], and offloading the medial foot (or in other words, shifting loading laterally) [20, 27].

1.2.3 Patient-Specific Computational Foot/Ankle Models of AAFD

To create the foot/ankle models alluded to in Section 1.2, patient-specific magnetic resonance images (MRI) were used to create approximately thirty solid bodies in SolidWorks 2007 (SolidWorks Corp., Concord, MA) representing the 3-dimensional bony anatomy of the foot for each of six individuals afflicted with AAFD. Additionally, using COSMOSMotion (Structural Research & Analysis Corp., Santa Monica, CA), five muscles were included in each model in the form of force vectors with magnitudes assigned as a percentage of patient body weight. Nearly 150 ligamentous structures were also captured in each foot/ankle model; these were incorporated as linear elements with assigned stiffness values. Those ligaments implicated in AAFD were assigned degradation percentages as per radiologist evaluation. Once each patient model was built (Figure 1.7), loading simulating single-leg stance was implemented and the resulting foot position was validated against patient-specific pre-operative radiographs [2, 11].

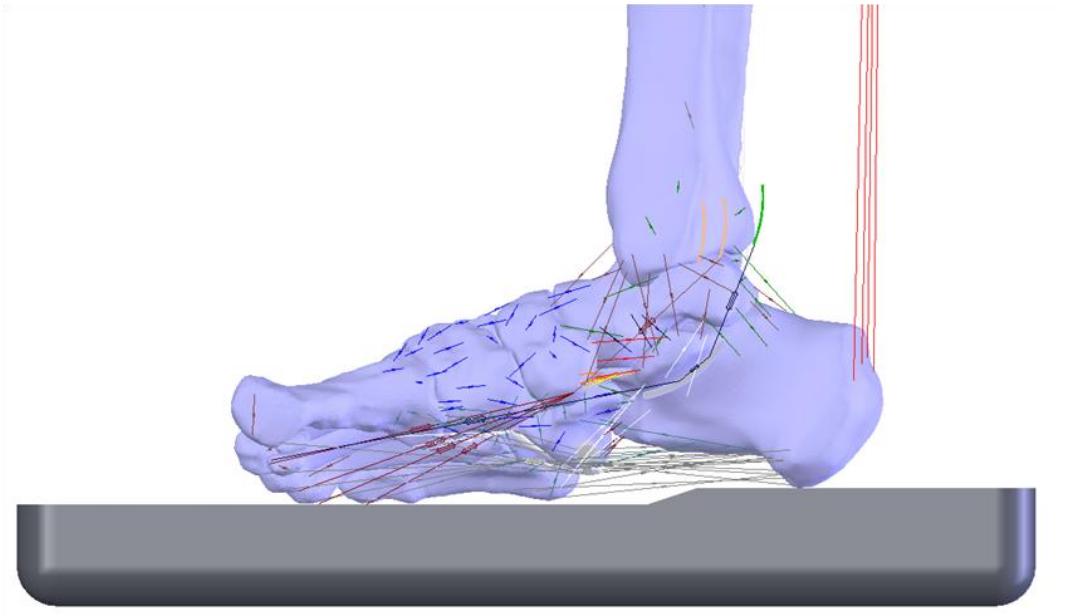

Figure 1.7: Pre-operative, Patient-Specific Model (right foot), medial view. This AAFD pre-operative model depicts musculature and soft tissue (represented as multicolored linear elements and vectors), as well as the bony anatomy, as it appears in the SolidWorks environment [11].

Post-operative foot/ankle models for five patients (one patient lost to follow-up) were developed similarly to the pre-operative models but included the patient-specific surgical correction (Figure 1.8). In the case of all five patients, a tendon transfer was performed in which the flexor hallucis longus (FHL) served to replace lost PTT function and a medializing calcaneal osteotomy (MCO) aided in both hindfoot valgus correction and medial offloading. Again, single-leg stance was simulated and resulting foot kinematics were evaluated against the patients' post-operative radiographs [11].

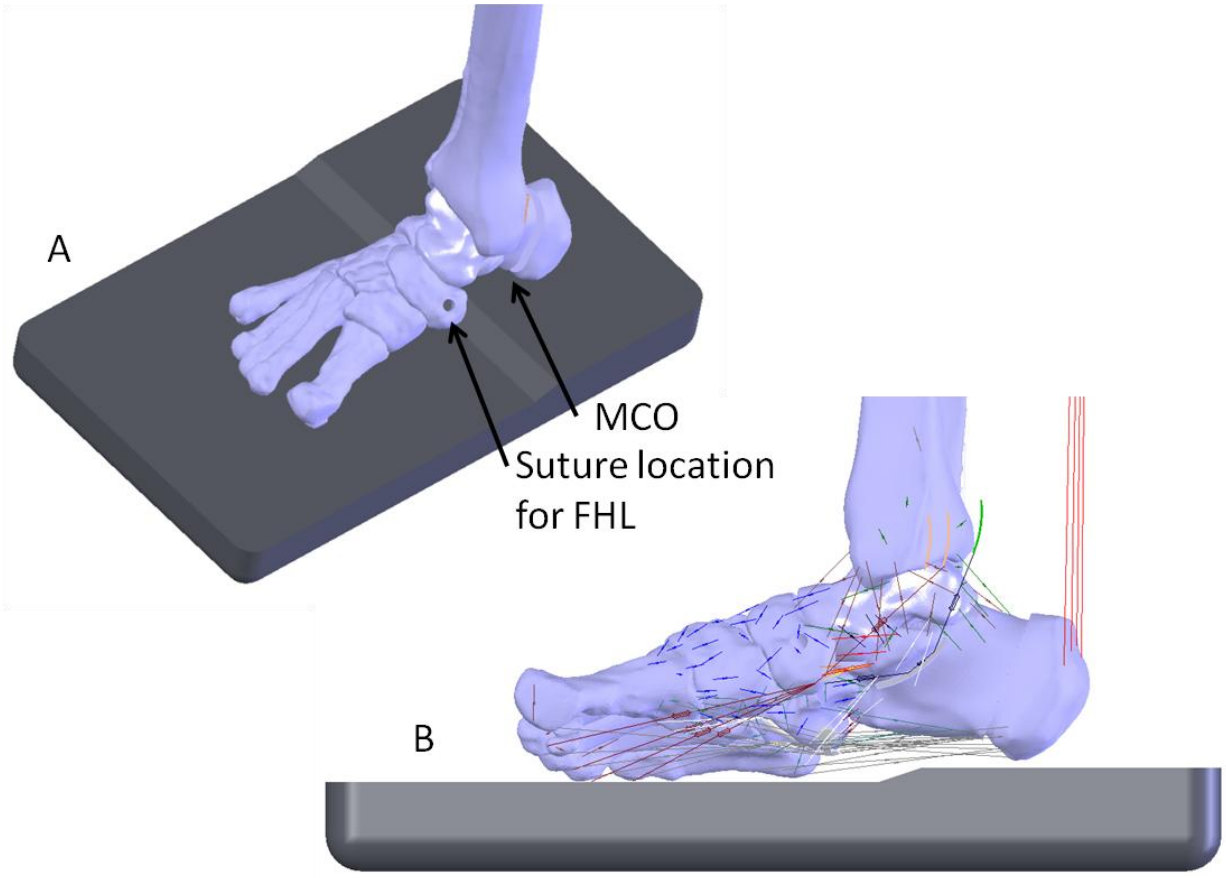

Figure 1.8: (A) Bony Anatomy with Surgical Correction (right foot). All patients received a flexor hallucis longus tendon transfer and medializing calcaneal osteotomy. The image shows the tunnel drilled into the navicular through which the tendon was looped and sutured, as well as the medially-offset posterior calcaneus. (B) Post-operative, Patient-Specific Model (right foot), medial view. In addition to the bony anatomy, this AAFD foot/ankle model depicts vectors and linear elements representing musculature and soft tissue [11].

Kinematic and radiographic comparisons consisted of assessing a total of fourteen measures, angles and distances, associated with AAFD that have been used clinically and found in literature [11, 32-33]. The angles were taken between reference lines of two anatomical (bony) structures or between the reference line of an anatomical body and that of a supporting base, while distances included bony heights taken relative to a defined reference line. Regarding both the pre- and post-operative cases, the computational models were found to have adequate agreement with the patient-specific radiographs [2, 11].

1.3 Informing the Structure - Function Relationship

For the models just described, bony and soft tissue properties, specifically ligament stiffnesses and muscle loading, were sourced from imaging and literature, respectively, and provided as inputs to the models [11]. This demonstrates how comprehension of bony and soft tissue anatomy, as well as the tissues' mechanical properties, informs the inputs and subsequent function of a given computational joint model. Generally, structure-function relationships have been investigated via cadaveric studies, imaging, and *in vivo* trials, the results of which can be coupled together to provide information about a given joint. For example, cadaveric dissection and imaging show how bony and soft tissues interact, while perturbation applied to these tissues during mechanical testing provides quantitative data regarding the tissues' strength and modes of deformation. Also, the movement of body segments relative to one another can be appreciated during patient trials like gait studies. Overall, these means of investigation help paint a more complete picture of normal joint mechanics, and in turn may reveal functional irregularities in diseased or injured states. Ultimately, this knowledge may then be incorporated into computational models, which would serve to further inform joint biomechanics.

While the above methodologies aid significantly in the study of joint function, some difficulties do exist in their employment. For example, cadaveric studies allow for catastrophic testing only; and therefore, larger sample sizes of a particular tissue are required in order to garner meaning from the study, but these larger quantities can be costly and difficult to obtain. Furthermore, although data is available for many anatomical structures, some tissues are not adequately described within the literature and so these

tissues are often assigned properties of similar structures. The ability to capture mechanical properties like stiffness may be limited due to tissue size or inaccessibility. With regard to muscle forces, direct measurements are nearly impossible to obtain; and therefore, literature often provides approximations of muscle contractions associated with a particular activity. Additionally, data for any single patient is unavailable and so these data are often reported as a range of values or as an average demonstrating a large variation. It is unclear as to which value from within this wide range should be assigned to a patient's computational model. How, then, can one contend with these difficulties such that the computational model is supplied with adequate input data to predict an appropriate response? While the approach of using literature-defined values provides a good first approximation of soft tissue parameters to be incorporated into a computer model, more finely-tuned parameters may strengthen the computer model's behavior. Because obtaining a better definition of tissue properties like stiffness cannot be determined via cadaveric testing or from human subjects, another methodology to determine such properties was sought.

1.4 Artificial Neural Networks

Artificial neural networks (ANNs) represent a type of machine learning in which the relationship between two or more quantities is "learned" by detecting patterns among known data. The characteristics of such relationship may not be fully defined or well understood; however, ANNs decipher a system's characteristics from known data via a training process [34-35]. By applying a learning algorithm, the system weights are continually updated until a particular goal is met or cost function is satisfied [35-37].

Finally, the ANN is able to apply the learned knowledge to other similar, never-before-seen data [35-36, 38-39].

1.4.1 General Neural Network Structure

Structurally, ANNs are comprised of several processing units, also known as neurons or nodes, which are interconnected in layers [34, 36, 38, 40-41]. In ANNs such as feedforward networks (Figure 1.9A), the neuron sums weighted inputs along with a bias and then passes that sum to a transfer (or activation) function before providing an output [36]. Various transfer functions exist, for example linear, piece-wise, or sigmoidal [36, 42-43], but generally, they serve to limit the output of the neuron within a certain range [36]. In the case of a radial basis function network (Figure 1.9B), inputs are not weighted prior to passing through the transfer function. Rather, they are compared to a pre-determined value known as a "center" using a distance function and then passed through a radial basis function, such as a Gaussian function (another type of activation function), whose width is determined by a shape parameter (σ) [36, 44].

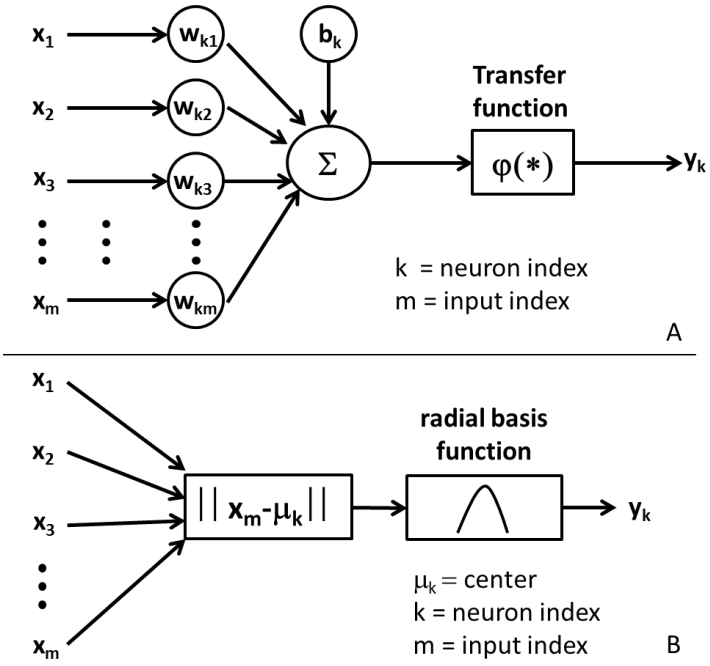

Figure 1.9: Neuron schematics. (A) Neuron model for a feedforward multilayer network where x_m = inputs, w_{km} = weights, b_k = bias, and y_k = output. Weighted inputs and a bias are summed together prior to being passed to a transfer function. An output from the neuron is provided from the transfer function. (B) An RBFN neuron does not weight inputs. Instead these are passed to a distance function and then to a transfer function, such as a Gaussian function. Adapted from [36].

As previously mentioned, several neurons may appear together in layers to create the network architecture (Figure 1.10). The simplest architecture is the single layer feedforward network in which inputs are directly connected to single layer of output nodes. (It is important to note here that a single layer refers to a computational layer; and therefore, inputs do not constitute a layer within an ANN.) A multilayer feedforward network is one that contains inputs and an output layer with at least one hidden layer between them [36]. The previously mentioned radial basis function network is an example of a multilayer feedforward network as it contains exactly one hidden layer [45]. Finally, a recurrent or feedback network is one that contains a feedback loop such that the output of one layer is connected to a preceding layer(s) or input(s) [36].

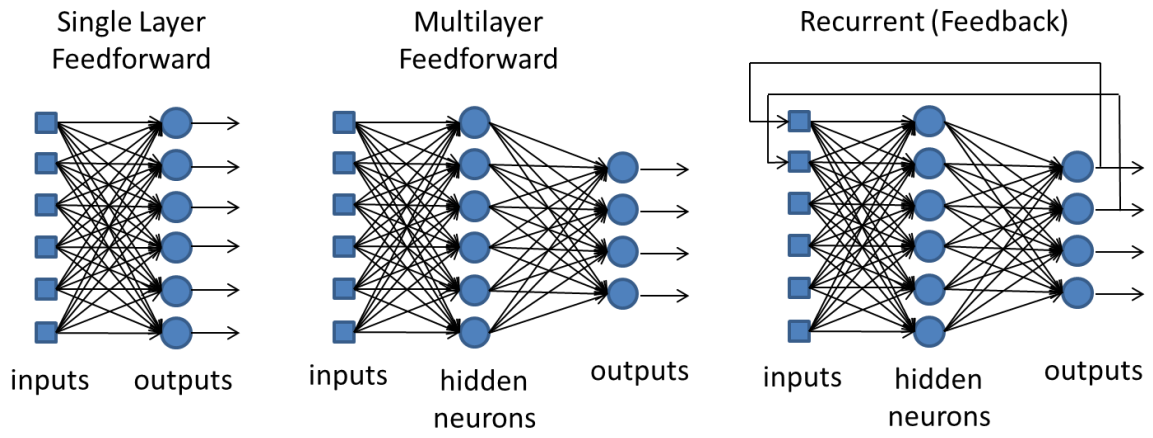

Figure 1.10: Network architectures. The simplest structure is the single layer feedforward network which simply passes inputs to the output (computation) layer. Additional layers (hidden layers) and feedback loops may be added to decipher additional data features for more complex problems. Adapted from [36].

Hidden neurons are those neurons which appear in a hidden layer, and the inclusion of one or more hidden layers serves to further elucidate characteristics among more complex input-output relationships like those that are not linearly separable [36, 45]. Both the number of hidden neurons and hidden layers may vary depending on the application as there is no pre-determined rule regarding how many of either should constitute the network architecture; however, it has been shown that a multilayer feedforward network with a single hidden layer should theoretically be able to solve any posed problem provided adequate training [34, 45].

1.4.2 Learning Rules

Ultimately, once architecture is determined, the ANN utilizes an iterative process in which a learning rule is used to minimize the error between a target value and its own prediction of that target [35, 37]. In the case of the feedforward network, error minimization is accomplished via backpropagation to adjust layer weights. Here, the cost function represents the error between the target (a constant value) and the ANN output,

which is equal to the summation of weighted inputs. Therefore, the minimization of error is accomplished by taking the derivative of the cost function with respect to the ANN output. However, since the neuron's output is dependent on the weight coefficients assigned to the inputs, the derivative of the cost function is essentially dependent on (i.e. taken with respect to) the weights. When the cost function is plotted against the weight coefficients, an error surface is created in which the minimum value of the surface is sought. Weights are adjusted such that a move along the error surface is made in the direction of the negative gradient of the cost function. This process is repeated until a minimum solution to the problem is determined. In the case of an ANN containing multiple layers of neurons, the error due to the overall network output is propagated backwards through all preceding layers such that weight adjustment occurs as a result of descending along the error surface toward a minimum solution [46-47].

Regarding the radial basis function network, weights belonging only to a single layer are to be determined, and this determination is carried out in a more direct, single-step procedure. A pseudo-inverse is used to calculate the output layer weights that best minimize the cost function. The need to use the pseudo-inverse arises from the fact that the number of unknowns outnumber the equations available for solving; and therefore, the problem at hand effectively transforms into solving for an approximate (rather than exact) network output [48].

1.4.3 Training Methods

In order for an ANN to learn, known data is presented to the network following its subdivision into two sets. The first subset is known as the training set and comprises a

majority of the total known data from which the network can extract features and determine an input-output relationship. After a single epoch, or iteration, in which all of the training data is presented to the network, the network's final output(s) is (are) compared to the target data. Based on the minimization criteria, system weights are adjusted and the training data is presented to the network once more. This process continues such that the training data is repeatedly presented to the network over many epochs until the error on the training set is minimized [43]. Subsequently, the second subset, which is called the test set, contains the remainder of the known data, and has yet to be seen by the ANN, is presented to the network. The purpose of this second set of data is to provide a true estimate of network performance on similar, unseen data as the training performance tends to be optimistic due to the presence of noise [36, 45, 49].

The training data can be furthered divided to make use of a validation set, which is smaller than the training subset and acts as another means to stop training. Similar to the test set, the validation set also provides an idea of network performance; however, this performance check occurs during the course of training. Although training error may continue to decrease, validation error may initially decrease and then begin to rise for several consecutive epochs. This rise in error indicates possible overfitting (to be discussed later) of the data and thus training must be halted at the point just prior to the increase in error; parameters associated with this point are chosen for the network [34, 36, 43, 45].

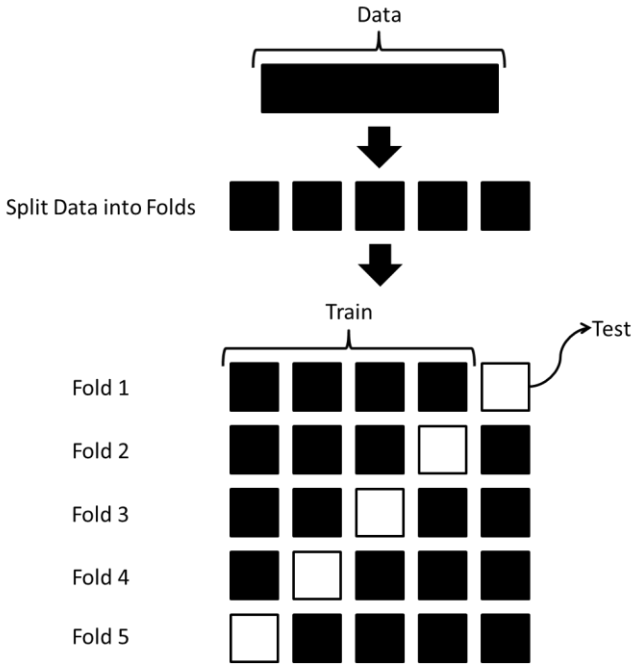

Figure 1.11: Cross-validation. Data is first split into K-folds (in this case, 5 folds). A single fold is removed and used as test data, while the remaining data constitutes training data. Following learning, the test fold is placed back into the overall data and a second fold is removed; again, learning takes place. This process continues until all folds have been left out of the training group at least once. Adapted from [36].

Another technique utilized in training networks is cross-validation (Figure 1.11). This method makes use of all of the known data by first splitting the data into two groups. The first group, the training subset, is used to train the network, while the second group, the test subset, is used to determine the performance error. Following this, the test subset is placed back into the overall data, and a new split of training and test data is used to train the network. Once this process is repeated for all folds, the performances for all test subsets are averaged to provide a final performance error for the network. The key benefit of cross-validation is that all data is presented to the network as training data at some point in the training process and likely presented as such multiple times [34, 36, 49-50]. This eliminates any guesswork as to which data should comprise training versus test subsets.

Generally speaking, the aforementioned training processes impact a network's ability to generalize, or determine a plausible output for never-before-seen data based on what it learned during training [36, 45]. Too little training results in the network learning the training data incompletely, i.e. underfitting the data, and subsequently generalizing poorly when given new data. Like underfitting, overfitting also results in the same poor generalization abilities; however, this phenomenon is the consequence of a network matching the training data (including noise) so well that it cannot determine outputs for new data that fall just outside of the target data [34, 36, 45, 49]. In other words, the network may predict well for only the exact values encountered in training but provide potentially inaccurate predictions for a value never presented during training.

The above examples also highlight a notable feature of artificial neural networks. Networks are useful for interpolating among data rather than extrapolating [45]. While a network will provide a prediction for any input presented to it, the validity of that prediction should be considered in the context of the problem statement and the range of the training data. Outliers may require further investigation [45]. To counter any of the issues just described, multiple rounds of training may be performed and/or more data may be presented to the network to ensure optimal network performance [43, 45].

1.4.4 General Uses and Applications to Biomedical and Biomechanical Models

Given their learning capabilities, ANNs are useful for several reasons. As stated in the preceding section, neural networks have the ability to generalize based on knowledge garnered from training on known data. Because of this, little needs to be known *a priori* about the input-output relationship [36]. Furthermore, ANNs may be applied to more

complex input-output relationships, including those that are nonlinear [36, 45, 51]. They may be applied to a wide range of problems including, but not limited to, classification, pattern recognition, function approximation, and image recognition [35-37, 39, 51-59].

Because they can lend themselves to such a wide variety of tasks like those just mentioned, artificial neural networks have been used in various fields from banking and economics to biomedical fields like pharmaceutics and biomechanics [3, 35-37, 42, 45, 52-55,60-62, 63]. Regarding the latter biomedical examples, Agatonovic-Kustrin et al. used ANNs to determine the component concentrations comprising an antihistamine tablet. Specifically, particular spectral patterns were identified within a spectral analysis of the ranitidine hydrochloride tablet thus distinguishing certain components [35]. In another study using ANNs, Ahmed presented several examples in which networks predicted survival among cancer patients by drawing a relationship between survival and input data like age, gender, and symptoms [52]. Musculoskeletal applications have also been identified among the neural network literature and include studies like those conducted by Lu et al. In this work, the investigators sought to determine cartilage stresses in a modeled knee. Two additional biomechanical studies were conducted by Eskinazi and Fregly [53] and Kaufman et al. [60]. In the former example, Eskinazi and Fregly used ANNs to predict contact between the femoral component and tibial plateau of a knee implant, while in the latter example, Kaufman et al. simulated both intact and fractured bone via an electrical model and employed neural networks to classify different levels of fracture healing.

1.4.5 Preliminary Neural Network Study

Based on the applications found in literature, a preliminary neural network study was initiated for ligament stiffness optimization. In this study, a single patient-specific pre-operative AAFD model was used to generate forty datasets of kinematic-stiffness pairings; these served as training data for the ANN. A single kinematic input consisted of four elements representing navicular height (mm), 1st cuneiform height (mm), talo-1st metatarsal angle (degrees), and talo-navicular angle (degrees), while a single output consisted of thirty-two ligament stiffness values (all belonging to the AAFD-afflicted ligaments). A feedforward network with a single hidden layer and ten hidden neurons was implemented within MATLAB, and the forty known datasets were randomly divided into training (70% of data), validation (15%), and test (15%) subsets [64].

Mean squared error curves were observed, and as expected, error on the training set reached a lower minimum than that on the validation and test sets. The latter two groups of data had similar shapes and no sudden increases in error were observed (which would have indicated overfitting of the data). Additionally, correlation (R) values between predicted and target ligament stiffnesses on all three data subsets were ≥ 0.95. Finally, when the trained feedforward network was provided with the original computer model's kinematic measures, it predicted all thirty-two ligament stiffnesses within 4.7% of the originally assigned ligament stiffnesses for that patient-specific model [64].

1.5 Objective

Given the manner in which artificial neural networks work, their applications in the biomedical field, especially within biomechanics, and the promising results of the preliminary study presented above, ANNs were considered a suitable means to further

study the foot/ankle complex. Again, computational models are limited by the inputs they receive; and therefore, improving the supplied inputs may enhance the computer model's performance. This statement is one that applies to the existing foot/ankle models used by the ORL to study AAFD. While these models perform well, their predictive ability can be improved further; and thus, the objectives of the current work are as follows:

(1) For a single patient-specific model, use both feedforward and radial basis function artificial neural networks to predict more finely-tuned ligament stiffness values for those ligamentous structures implicated in Adult-Acquired Flatfoot Deformity, and

(2) Improve the predictive capability of that single patient's pre- and post-operative computational foot/ankle models.

CHAPTER 2 Methods

2.1 Predictions for Pre-Operative Foot/Ankle Model

In order to provide optimized ligament stiffness inputs for the computational foot/ankle model and determine whether these optimized values would result in an improved foot/ankle model performance, four major tasks were implemented (Figure 2.1): (1) kinematic measures of interest were selected, (2) kinematic datasets were generated for the ANNs, (3) two types of ANNs were developed and trained, and (4) the kinematics of the computational foot/ankle model were measured following application of the ANN-generated stiffness predictions and compared to the patient radiographic measures. To complete the first task, both clinical preference and correlation between computational model and patient radiograph were considered in selecting measures. Specifically, two distances and two angles with the high correlations between computational model and radiograph in [2, 11] were selected as measures of interest. These measures (Figure 2.2), which included both talo-navicular and talo-1st metatarsal angles (degrees) and navicular and 1st cuneiform heights (millimeters), were measured and recorded during the second task of data generation.

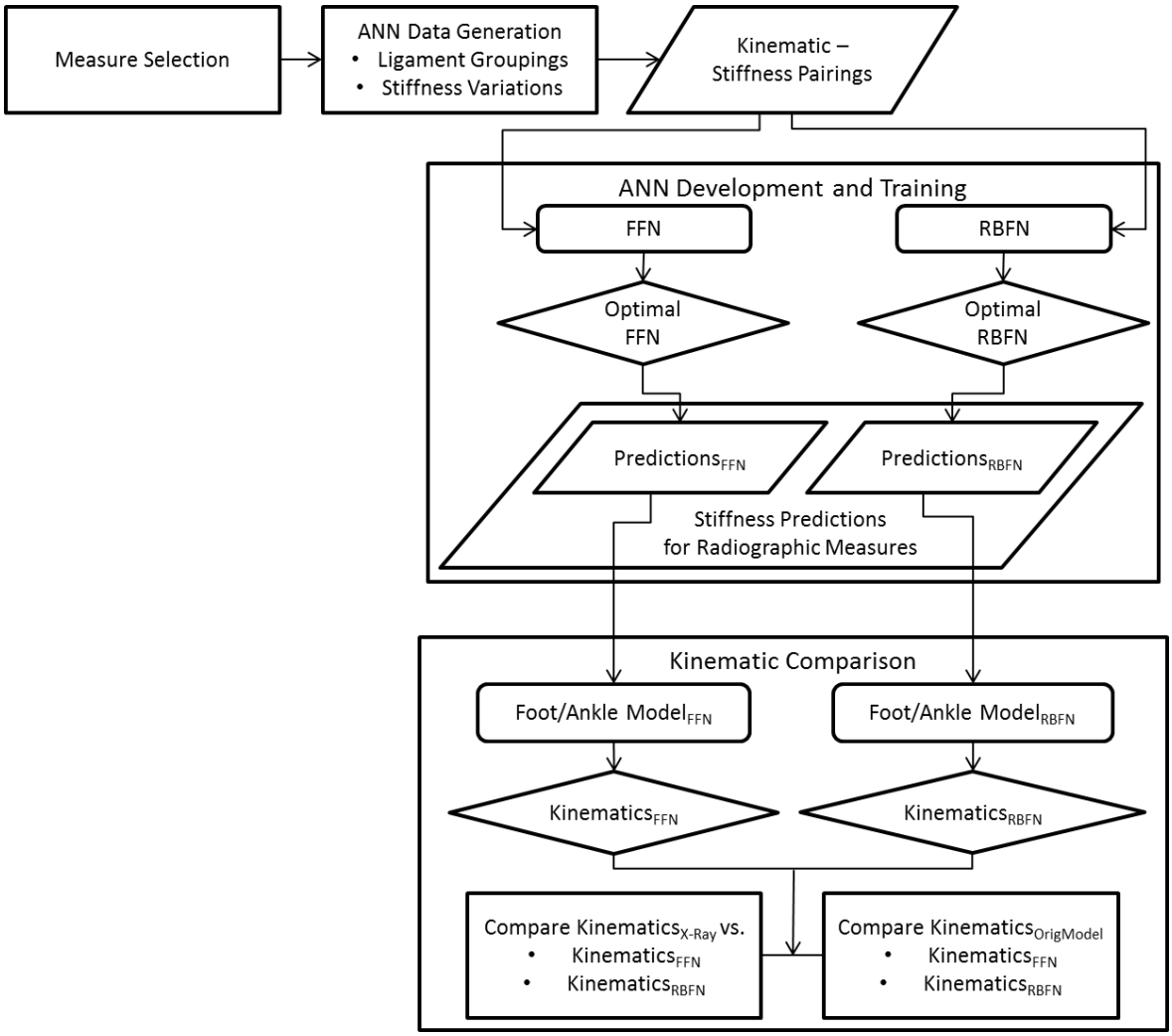

Figure 2.1: Task Flow. The four major tasks completed during this research are depicted above along with their key subtasks.

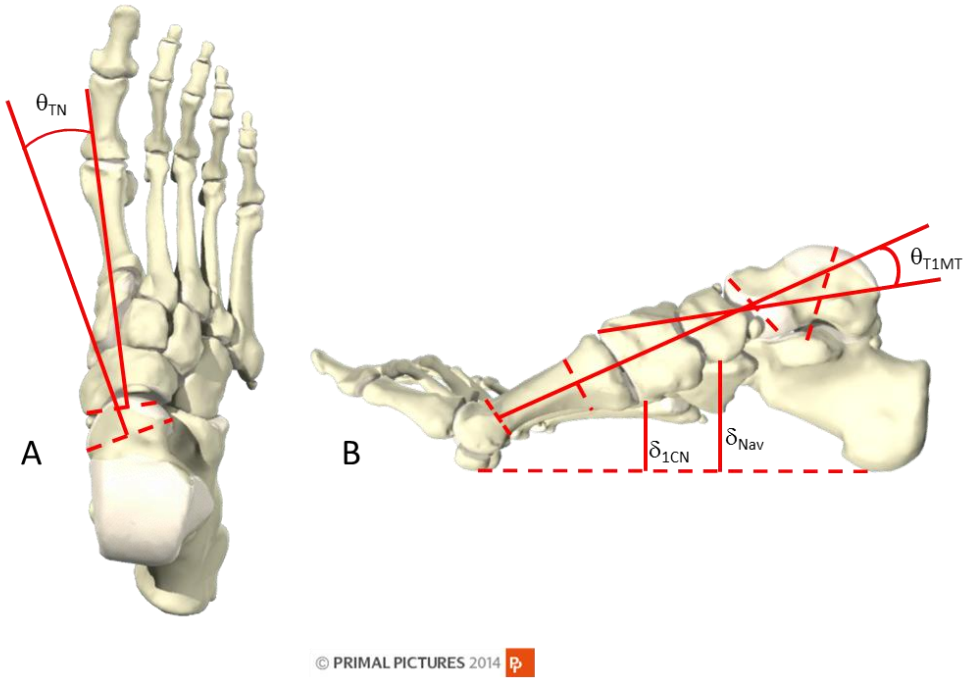

Figure 2.2: Kinematic Measures (right foot). (A) θ_{TN} = talo-navicular angle, oblique AP view. (B) θ_{T1MT} = talo-1st metatarsal angle; δ_{Nav} = navicular height; δ_{1CN} = 1st cuneiform height, medial view. [Adapted from: Primal Pictures for Anatomy TV and 2, 11.]

For the second task, a single pre-operative, patient-specific foot/ankle computer model (patient 3, or P3) developed during previous work [2, 11] was used as a foundation for the current research. To generate kinematic datasets for ANN training, the AAFD-afflicted ligamentous components were first assigned to one of three groupings—medial, plantar, or spring—generally based on location (e.g. deltoid components were assigned to the "medial" group), and the magnitude of the ligament stiffnesses in each of the groupings were varied individually or in combination with one another. A total of fourteen ligament stiffness values were varied (Table 2.1). Individual variations were carried out in five percent increments, up and down, from both the attenuated values originally assigned to the P3 model, as well as from the "normal" ligament values; resulting kinematics from the model were recorded. Variations were created in this way to capture a more representative

range of kinematic data for the P3 foot/ankle model specifically because ANNs require a wide range of data for better generalization [45]. As a result, a total of 173 datasets were generated for ANN training. It is important to note that, while stiffnesses and kinematics represented inputs and outputs, respectively, for the computational model, the input-output definition for the ANNs was reversed; thus the 173 datasets were comprised of kinematic-stiffness pairings. Furthermore, from an anatomic perspective, some of the varied ligaments have multiple bands or greater widths, so several linear elements represented them within the foot/ankle model (Table 2.1). For most of these cases, linear elements belonging to the same ligament were assigned the same stiffness value [11], and thus the same amount of variation. A total of thirty two linear elements and fourteen unique stiffness values comprised the AAFD-afflicted ligaments.

Ligament	No. Linear Elements	Stiffness (N/mm)	
		Attenuated	Normal
Tibiocalcaneal	2	75.00	200.00
Tibionavicular	2	5.00	40.00
Tibiospring 1	1	7.63	61.00
Tibiospring 2	1	25.00	200.00
Anterior Tibiotalar*	1	90.00	90.00
Posterior Tibiotalar*	2	117.00	117.00
Talocalcaneal Interosseous	3	33.75	90.00
Plantar Fascia 1	5	30.00	40.00
Plantar Fascia 2	1	45.00	60.00
Plantar Fascia 3	2	37.50	50.00
Plantar Fascia 4	2	15.00	20.00
Plantar Fascia 5*	2	150.00	150.00
Spring 1	2	16.88	45.00
Spring 2	6	2.29	18.30

Table 2.1: Starting Values, Ligament Stiffnesses. To generate ANN training data, ligament stiffness values were varied from both the attenuated and normal stiffness values listed above [11]. Those components denoted with (*) retained the normal stiffness value or received a "0" grade (i.e. no noticeable attenuation) per the clinician's evaluation in the original P3 model [11], but were included during data generation here due to their anatomic proximity.

For task three, predicting ligament stiffnesses falls under the function fitting task in ANNs and so the kinematic-stiffness pairings were used to train both feedforward and radial basis function networks. A feedforward network (Figure 2.3) with a single hidden layer, two inputs, and fourteen outputs was created in MATLAB R2015a (The MathWorks, Inc., Natick, MA) using the Neural Network Toolbox. Inputs included both the talo-1st metatarsal angle (T1MT) and the talo-navicular angle (TN); however all four kinematic measures were still measured for comparison among model predictions. While all four measures were initially recorded, it was determined that ANN training would be carried out with only the talo-1st metatarsal and talo-navicular angles for two reasons. First, whereas the two heights are both in the sagittal plane, the two angles exist in two different planes (sagittal and transverse). This representation of the two planes was desirable over utilizing measures strictly from one plane. Further, it was noted that height measurements obtained from dataset generation did not capture a wide enough range such that appropriate height data could be supplied to the neural networks during training. However, this was not the case for angular measures as dataset generation did, in fact, produce an appropriate range of data encompassing radiographic measurements. Therefore, it was determined that ANN training would be carried out with only the talo-1st metatarsal and talo-navicular angles, and the two remaining heights would be monitored to ascertain whether any computational model improvements resulted due to the inclusion of ANN-predicted stiffnesses.

A ten-fold cross validation scheme was implemented in combination with MATLAB's feedforwardnet function, which randomly distributed the training data into

three subsets: training, validation, and test. The cycling of all datasets through the cross-validation scheme was accomplished with an "if/else" statement [50] that was embedded within a pair of "for" loops. Within the internal loop, the number of hidden neurons was varied from one to ten to determine the optimal network size, while the external loop cycled through ten states (0 through 9) to establish the best starting point for the random number generator.

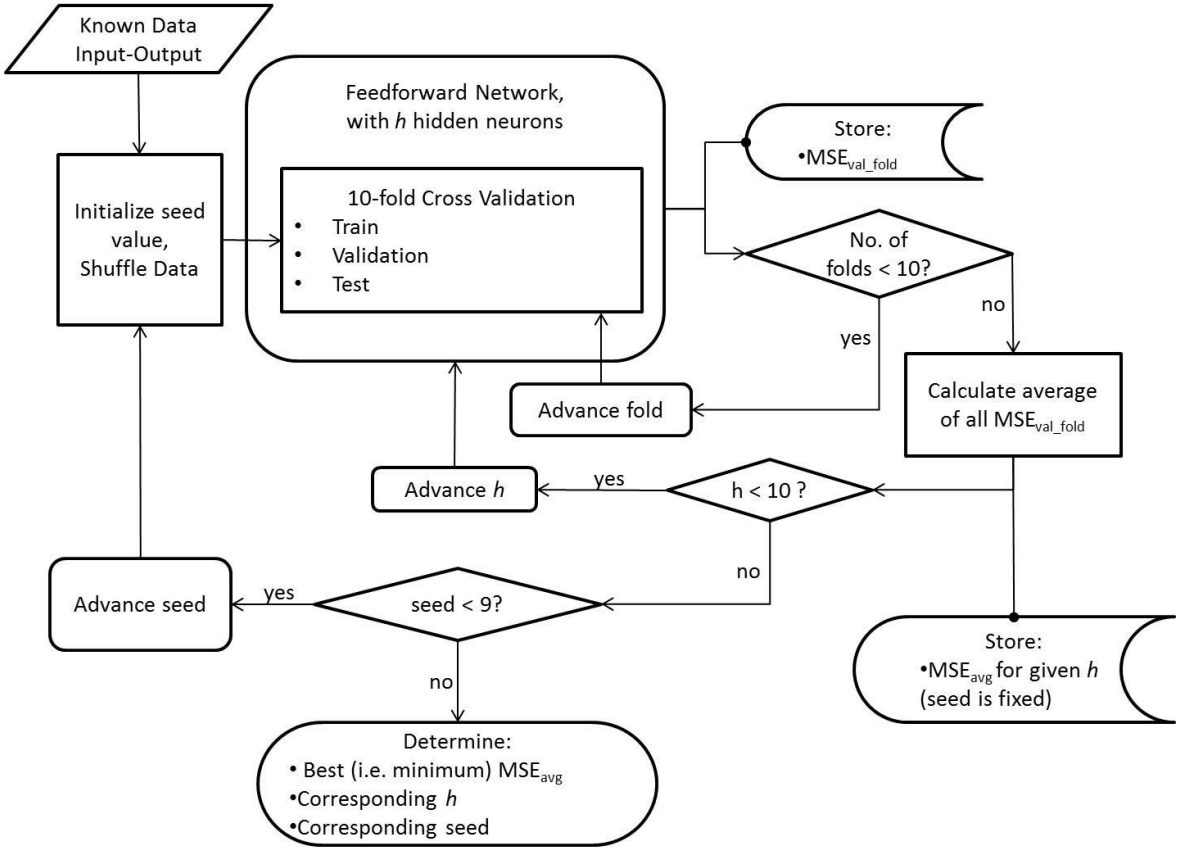

Figure 2.3: Feedforward Network. A series of "for" loops containing a cross validation scheme determined the optimal stiffness for the fourteen ligaments of interest.

When training networks within MATLAB, the state of the random number generator (RNG) determines the initial weights used during network training as well as the random division of data performed by MATLAB functions like feedforwardnet [65-66].

The state of the RNG is dependent on its "seed" value and where along the seed the RNG last stopped. Every time a network is re-trained, a new set of initial weights is assigned to the network and is dependent on the progression of the RNG within that seed. Per Dr. V. Kecman, the RNG can be visualized as a circular wheel with major tick marks representing the various seeds (Figure 2.4). Minor tick marks represent the random values within that seed. If a network is trained with five initial weights, the first five values of the chosen RNG seed will be used. When the network is re-trained, the next five values will be chosen, and so on. In this way, it is unclear as to where the RNG starts and stops. To avoid this issue and be able to reproduce network results, the seed was fixed such that the starting point of weight selection was consistent [65-66]. In the current work, multiple seeds were investigated to increase the likelihood of obtaining a favorable data division and weight selection for each network, thus requiring (1) initialization of the seed both inside and outside the "for" loops and (2) the external "for" loop to pass through various seeds (i.e. 0-9) during the network training process.

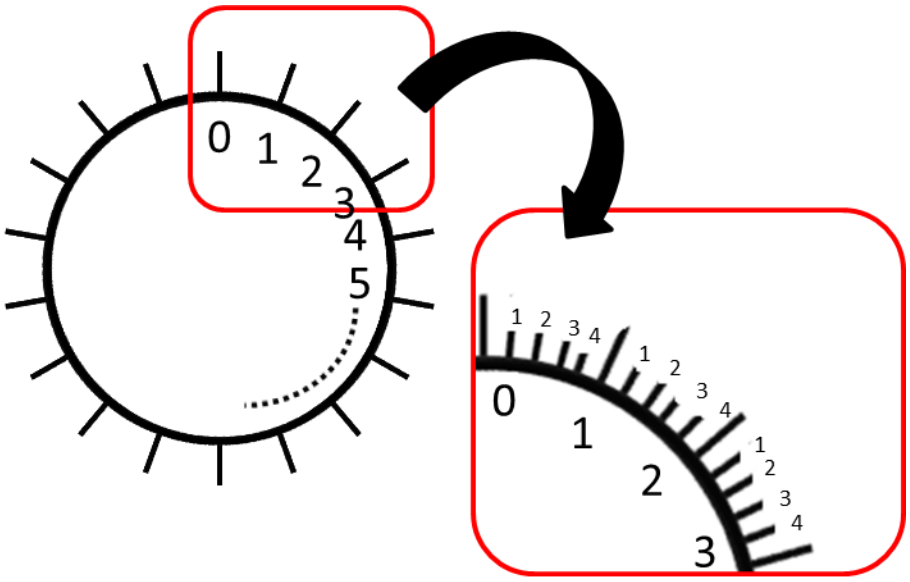

Figure 2.4: Random Number Generator. The RNG can be illustrated as a wheel with the larger tick marks representing seed values. The smaller numbers within the inset image represent individual, random weight values that are applied to the network. Each seed has a different order of infinite random values within it, though only four are depicted per seed for illustrative purposes [Description garnered from conversation with Dr. V. Kecman].

Beginning with a RNG state of 0 and a single hidden neuron, the feedforwardnet function randomly distributed the generated datasets into training, validation, and test subsets. Network performance was assessed using mean square error (MSE), given in Equation 1, where *N* represents the number of datasets, *t* is the target value (i.e. stiffness), and *a* is the ANN-prediction [43, 59, 67]. Prior to further elaborating on the network selection process, two additional comments must be made regarding MSE. First, error is minimized as the ANN predictions get closer to their respective target values, thus MSEs closer to 0 represent better network performance. Secondly, due to the summation present in Equation 1, MSE tends to favor larger target values when the scale of the training examples varies. To decrease this effect, input-output data was standardized within a range of [-1, 1] prior to supplying it to the network [43, 61]. Following selection of the

optimal network out of those networks trained, data was post-processed to transfer final predictions back into the original units (i.e. degrees for kinematics measures, N/mm for stiffnesses).

$$MSE = \frac{1}{N}\sum_{i=1}^{N}(t_i - a_i)^2 \qquad (Equation\ 1)$$

For each combination of RNG and hidden neuron number, MSE on the validation set was stored for every fold and then averaged. The hidden neuron number was increased by one and then the cross-validation process was repeated; this process continued until ten hidden neurons were tested for the given RNG state. Once all hidden neurons had been cycled through, the minimum average validation was stored, and then the RNG state was increased to one and the aforementioned processes were repeated. In summary, a total of ten RNG states were tested, and ten different hidden neuron numbers were tested under each RNG state for a total of 100 average validation performances. These 100 were narrowed down to the ten smallest MSE values, one per RNG state, and the network associated with the minimum of these ten values was determined to be the optimal network out of those networks explored. The corresponding RNG and hidden neuron number were noted, and subsequently, the performance error on the test set was also reported for the optimal network, as were the performance and the correlation (R) values on the entire dataset. Lastly, this optimal network was used to make ligament stiffness predictions for the patient-specific radiographic data.

Alongside the feedforward network, an optimal radial basis function network was also determined using a cross-validation procedure (Figure 2.5). Here, the RNG state

(required to shuffle or randomize the data prior to its pass through the cross-validation scheme), *k*, the number of centers, and σ, the shape parameter were cycled through and optimal values for each determined. Similar to the FFN process, data was divided into training, validation, and test subsets; these subsets were then supplied to a custom function code calling a radial basis function network developed and provided by V. Kecman, PhD [68] and MSE on the validation set was calculated. Once MSE was determined for each fold, the MSEs for all folds were averaged and stored; this value represented the average MSE for a given σ and k combination. σ was then advanced while k remained fixed and the above process was repeated. Once all shape parameters were tested, k was advanced to create a new set of networks. The minimum validation performance of all σ and k combinations was stored for the given RNG state; this procedure continued until a minimum validation MSE was recorded for each seed value (i.e. ten total performance numbers). Finally, the network corresponding to the smallest of these ten values was chosen as the optimal network, and the RBFN's associated RNG seed, number of centers, and shape parameter were saved. (Because the quantity of centers determines where among the data a Gaussian function should be placed, the number of centers also defined the number of hidden neurons.) As with the optimal FFN, the test set error, overall data performance and correlation values were noted. Finally, ligament stiffness predictions were made based on the patient-specific radiographic data.

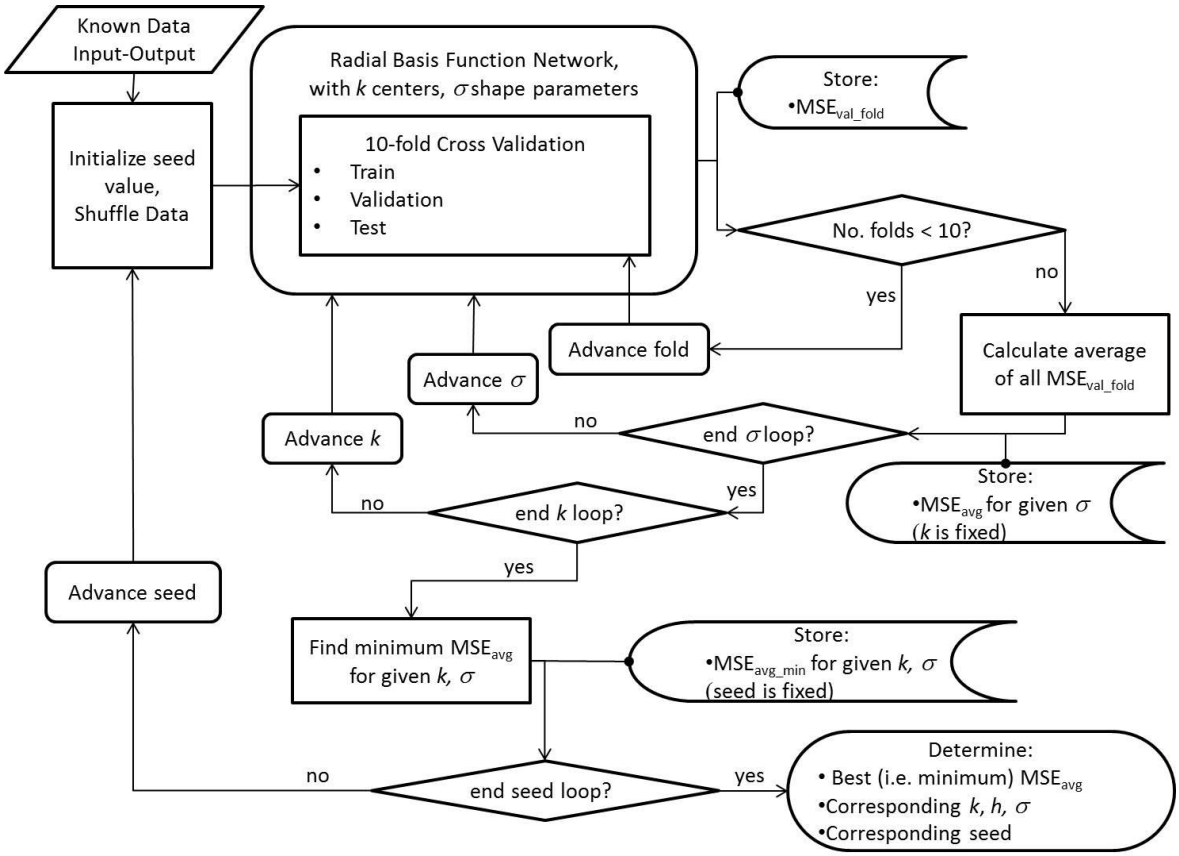

Figure 2.5: Radial Basis Function Network. A cross validation scheme was used to determine the number of centers and shape parameters, and ultimately the optimal stiffness, for the fourteen ligaments.

For the fourth and final task, two computational foot/ankle models were established; one utilized the stiffness predictions from the FFN while the second used stiffness predictions from the RBFN. For those ligaments represented by more than a single linear element within the computational model, the ANN-predicted stiffness was applied to each linear element belonging to that ligament. The resulting kinematics of these two foot/ankle models were compared to one another, as well as to the kinematics of the existing foot/ankle model, using a simple percent difference relative to the patient-

specific radiographic values to determine whether predictions from either network enhanced the predictive ability of the existing foot/ankle computational model.

2.2 Predictions for Post-operative Foot/Ankle Model

Stiffness prediction for the post-operative model was carried out in the same way as that for the pre-operative model. Regarding the existing post-operative model, the major differences between it and the pre-operative foot/ankle model involved the capture of the patient-specific surgical corrections: a medializing calcaneal osteotomy along with a FHL transfer. Attenuated ligament values were assigned the same values as the pre-operative state [11]; and therefore, variations were carried out in a manner similar to that used for the pre-operative model when generating datasets for ANN training (here, N = 160). Following training of the neural networks, the resulting kinematics from the foot/ankle models using the ANN-predicted stiffnesses were compared to one another, the existing post-operative patient-specific model, as well as to the patient-specific post-operative radiograph.

2.3 Effect of Stiffness Variation on Angular Measures

The main objectives of this work centered on the optimization of ligament stiffness inputs for the foot/ankle computational models of a single patient. As a compliment to the main studies listed above, a secondary analysis was completed on a portion of the generated data to observe the effects of stiffness variation on kinematic measures. Specifically, ligament groupings that were varied independently of the remaining two groups were examined to determine whether a percent change in stiffness variation created a noticeable change or trend in T1MT or TN. In other words, the slope of a line fit to the

kinematic data was tested to see if it differed significantly from zero. Variations from both attenuated and normal values were observed separately. A t-statistic was used and p-values below $\alpha = 0.05$ indicated a slope significantly different than zero, while plots displaying the equations of the trend lines demonstrated direction of trends.

CHAPTER 3 Results

3.1 Pre-operative Results

Stiffness variations were assigned to the foot/ankle model and resulted in 173 kinematic-stiffness pairings. Each dataset contained two kinematic measures, specifically the talo-1st metatarsal (T1MT) and talo-navicular (TN) angles, and these were sorted and plotted (Figure 3.1). T1MT and TN ranged from 13.71° to 30.52 and 14.04° to 29.18°, respectively. Variations were made from both attenuated and normal ligament stiffness values, and thus the data plotted represents a wide range of kinematic scenarios that the foot/ankle model was capable of simulating.

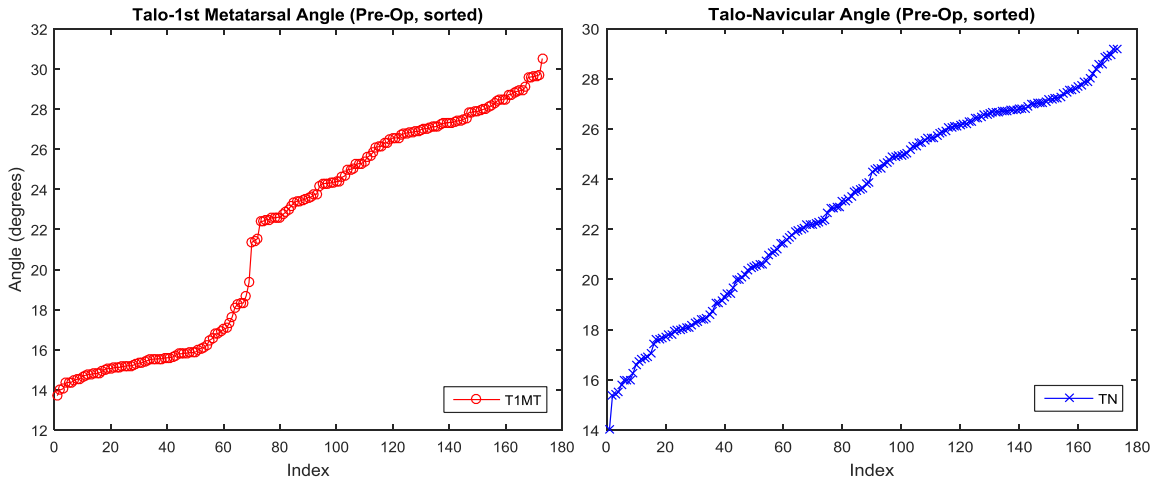

Figure 3.1: Pre-operative Angular Data. Talo-1st metatarsal (left) and talo-navicular (right) angles were sorted and plotted to illustrate the range of the ANN input data (N = 173). (Note: The horizontal axis represents the number of data points taken but does not represent matched pairs of T1MT and TN.)

Both feedforward and radial basis function networks were trained with the known kinematic inputs (talo-1st metatarsal and talo-navicular angles) from above and their corresponding outputs (ligament stiffnesses). Input and output data was standardized within the range of [-1, 1] prior to training. Of the networks trained, the optimal networks were those which resulted in the smallest mean square error (MSE) on the validation subsets (Table 3.1); their parameters are shown in Table 3.2. Additionally, performance of the optimal networks was observed on the test set, and both MSE and correlation (R) were calculated for the entire dataset (Table 3.1).

The optimal FFN resulted in a smaller MSE on the validation set than the RBFN, while the reverse was true for the test sets. When all 173 datasets were supplied to the optimal networks, the FFN's predictions of target stiffnesses resulted in a better MSE than the RBFN, while R values were similar for both networks. (Prior to calculating R values, data was first transformed back into the original units.)

	MSE			
Network	**Validation**	**Test**	**All Data (N = 173)**	**R (N = 173)**
Feedforward	0.034	0.084	0.040	0.98
Radial Basis Function	0.060	0.061	0.048	0.98

Table 3.1: Optimal Network Performance, Pre-operative Data. Mean square error (MSE) is shown for validation and test subsets, as well as for the entire data set. The optimal FFN and RBFN were chosen per the validation MSE, with test MSE demonstrating unbiased network performance. (Note: MSE was calculated for standardized data, which ranged from [-1, 1].) R, correlation between target and ANN-predicted stiffnesses, is shown for all data.

Following determination of the optimal networks, their corresponding parameters were output. The FFN resulted in an optimal network with 6 hidden neurons in the hidden layer, while the RBFN had 18 neurons. In the case of the RBFN, the values of the centers corresponded with the values of every k^{th} data in the training set; therefore, the number of neurons equated to N/k, and k was allowed to range from 1 to 80. σ, the shape parameter,

dictated the width of the Gaussian function; multiple values were cycled through with smaller and larger values representing wider, flatter and narrower Gaussian functions, respectively. Here, a value of 0.5 represented a wider Gaussian shape.

	Optimal Parameters			
Network	**RNG Seed**	**h**	**k**	**σ**
Feedforward	7	6		
Radial Basis Function	0	18	10	0.5

Table 3.2: Parameters Corresponding to Optimal Networks, Pre-operative Data. Ten seed values (0-9) were utilized during training; those resulting in the best performance are shown alongside other optimal parameters. h = number of hidden neurons; k = number of centers; σ = shape parameter.

To further investigate neural network performance, kinematics corresponding to the pre-operative model developed by Spratley [2, 11] were provided to the optimal neural networks, and these networks were used to predict the originally assigned ligament stiffnesses (Table 3.3). The largest percent difference seen among the FFN-predicted stiffnesses was just under 6.3%, while eleven of the fourteen RBFN-predicted stiffnesses fell under 7%. The remaining stiffness values were approximately 11.8% from their respective target values.

Ligament	Pre-Op Model Stiffness (N/mm)	FFN		RBFN	
		Stiffness (N/mm)	Percent Difference	Stiffness (N/mm)	Percent Difference
Tibiocalcaneal	75.0	76.1	1.45	80.2	6.93
Tibionavicular	5.0	4.7	-5.66	5.6	11.83
Tibiospring 1	7.6	7.2	-5.66	8.5	11.83
Tibiospring 2	25.0	23.6	-5.66	28.0	11.83
Anterior Tibiotalar	90.0	93.3	3.67	94.8	5.38
Posterior Tibiotalar	117.0	121.3	3.67	123.3	5.38
Talocalcaneal Interosseous	33.8	35.9	6.27	35.8	6.14
Plantar Fascia 1	30.0	31.8	5.91	31.7	5.75
Plantar Fascia 2	45.0	47.7	5.91	47.6	5.75
Plantar Fascia 3	37.5	39.7	5.91	39.7	5.75
Plantar Fascia 4	15.0	15.9	5.91	15.9	5.75
Plantar Fascia 5	150.0	158.7	5.82	158.4	5.63
Spring 1	16.9	17.7	4.67	17.0	0.74
Spring 2	2.3	2.4	5.63	2.4	3.29

Table 3.3: Target Ligament Stiffnesses (Pre-Op Model) vs. ANN-Predicted Stiffnesses. The optimal FFN and RBFN were used to predict stiffnesses for the pre-operative model. The predictions are shown alongside the pre-operative model's originally assigned stiffnesses, as well as their percent differences relative to these original stiffness values [11]. (Negative values represent an under prediction of the target value.)

Finally, the optimal networks were supplied with the radiographic kinematics and used to predict stiffnesses for this data (Table 3.4). Stiffness predictions made by both networks were reasonable and within the range of the training data. These predictions were then assigned as inputs to the computational foot/ankle model to determine whether kinematic performance improved due to the new stiffnesses; this kinematic comparison is illustrated in Tables 3.5-3.6. (As stated previously, in addition to the angles, two heights—navicular and 1st cuneiform—were also observed for any improvement. Though these were not included in the network, they were measured here due to their higher correlations among kinematic measures in [11].)

	Stiffness (N/mm)	
Ligament	**FFN**	**RBFN**
Tibiocalcaneal	107.7	86.9
Tibionavicular	7.9	4.7
Tibiospring 1	12.1	7.2
Tibiospring 2	39.6	23.7
Anterior Tibiotalar	125.0	110.5
Posterior Tibiotalar	162.6	143.6
Talocalcaneal Interosseous	44.8	47.9
Plantar Fascia 1	39.7	39.8
Plantar Fascia 2	59.6	59.7
Plantar Fascia 3	49.7	49.7
Plantar Fascia 4	19.9	19.9
Plantar Fascia 5	198.5	195.9
Spring 1	22.4	21.0
Spring 2	3.3	3.1

Table 3.4: Stiffness Predictions for Pre-Op X-Ray Kinematics. Patient-specific kinematics were introduced to each optimal ANN and the above stiffnesses were predicted. Predictions determined by both the optimal FFN and RBFN were within range of the training data, and in most cases, were similar to one another when compared on a component by component basis.

	Height (mm)		Angle (degrees)	
	Navicular	**1st Cuneiform**	**Talo-1st Metatarsal**	**Talo-Navicular**
FFN Model	12.12	7.72	18.41	26.42
RBFN Model	10.77	7.25	21.59	26.18
Pre-Op Model	9.68	6.76	25.29	24.78
Pre-Op Radiograph	15.26	10.79	20.15	24.49

Table 3.5: Pre-Operative Kinematic Measures. The ANN stiffness predictions corresponding to the patient-specific radiographic data was introduced to the computational foot/ankle model. Resulting kinematics are shown above in comparison to the pre-operative model developed by Spratley [2, 11] and the patient kinematics.

	Percent Difference			
	Height		Angle	
	Navicular	**1st Cuneiform**	**Talo-1st Metatarsal**	**Talo-Navicular**
FFN Model	20.58	28.45	8.64	-7.88
RBFN Model	29.42	32.81	-7.15	-6.90
Pre-Op Model	36.57	37.35	-25.51	-1.18

Table 3.6: Percent Difference Relative to Pre-Op Patient Radiograph. Three of four kinematic measures of interest were improved upon, in comparison to the pre-operative model, by stiffnesses provided by both networks. (Negative values indicate an over-prediction relative to radiographic measures.)

3.2 Post-operative Results

The steps detailed above for the pre-operative case were also completed for the post-operative case, and so corresponding figures and tables for the post-operative case are given below. Here, 160 stiffness variations were completed for the post-operative model and the resulting kinematics are depicted in Figure 3.2.

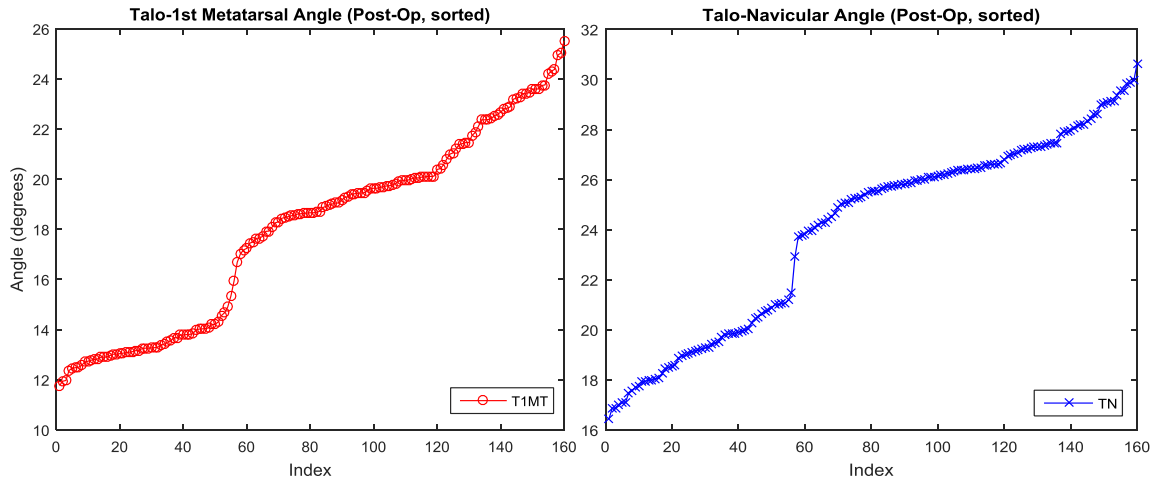

Figure 3.2: Post-operative Angular Data. Talo-1st metatarsal and talo-navicular angles from all 160 training data ranged from [11.77°, 25.52°] and [16.43°, 30.64°], respectively. (Note: As this data is sorted, T1MT and TN data falling along the same horizontal value are not matched pairs.)

Optimal networks were selected among the networks tested based on MSE of the validation subsets; MSE of the test subset and entire dataset, as well as R value of the entire dataset, were also recorded (Table 3.7). As in the pre-operative case, MSE on the validation subset was lower for the FFN than for the RBFN; the reverse was true for the test subsets. MSE on the entire dataset, as well as the R-values, were similar for both networks.

	MSE			
Network	**Validation**	**Test**	**All Data (N = 160)**	**R (N = 160)**
Feedforward	0.034	0.106	0.050	0.98
Radial Basis Function	0.072	0.072	0.057	0.98

Table 3.7: Optimal Network Performance, Post-operative Data. Mean square error (MSE) is shown for validation and test subsets, as well as for the entire data set. The optimal FFN and RBFN were chosen per validation MSE, with test MSE demonstrating unbiased network performance. (Note: MSE was calculated for standardized data, which ranged from [-1, 1].) Correlation (R) was calculated for the entire dataset.

	Optimal Parameters			
Network	**RNG Seed**	**h**	**k**	**σ**
Feedforward	8	7		
Radial Basis Function	0	16	10	0.5

Table 3.8: Parameters Corresponding to Optimal Networks, Post-operative Data. Ten seed values (0-9) were utilized during training; those resulting in the best performance are shown alongside other optimal parameters. h = number of hidden neurons; k = number of centers; σ = shape parameter.

Parameters of these optimal networks are shown in Table 3.8 and neuron numbers were similar to those found pre-operatively. As in the pre-operative case, the optimal networks were used to predict the originally assigned post-operative stiffness targets (Figure 3.9). Stiffness predictions from both the feedforward and radial basis function networks were within range of the training data.

	Existing	FFN		RBFN	
Ligament	**Stiffness (N/mm)**	**Stiffness (N/mm)**	**Percent Difference**	**Stiffness (N/mm)**	**Percent Difference**
Tibiocalcaneal	75.0	67.2	10.38	73.8	1.66
Tibionavicular	5.0	4.6	7.75	5.5	9.67
Tibiospring 1	7.6	7.0	7.75	8.4	9.69
Tibiospring 2	25.0	23.1	7.75	27.4	9.67
Anterior Tibiotalar	90.0	79.9	11.20	85.1	5.44
Posterior Tibiotalar	117.0	103.9	11.20	110.6	5.44
Talocalcaneal Interosseous	33.8	27.6	18.17	30.3	10.10
Plantar Fascia 1	30.0	25.2	16.10	24.9	17.09
Plantar Fascia 2	45.0	37.8	16.10	37.3	17.09
Plantar Fascia 3	37.5	31.5	16.10	31.1	17.09
Plantar Fascia 4	15.0	12.6	16.10	12.4	17.09
Plantar Fascia 5	150.0	126.6	15.58	121.5	19.00
Spring 1	16.9	17.0	0.60	16.7	1.06
Spring 2	2.3	2.5	8.83	2.6	13.74

Table 3.9: Target Ligament Stiffnesses (Post-Op Model) vs. ANN-Predicted Stiffnesses. Stiffness predictions and their percent differences relative to the assigned stiffnesses for the post-op model are shown.

Finally, the post-operative kinematics from the patient-specific radiograph were input to the optimal ANNs and new stiffnesses were predicted (Table 3.10); all predictions were reasonable and within range of the training data. As a result, these new stiffnesses were introduced to the computational foot/ankle model, and the associated kinematics were recorded (3.11) and compared (3.12) to those generated by the computational model developed by Spratley [11]. Again, two heights in addition to the two angles of interest were assessed.

	Stiffness (N/mm)	
Ligament	**FFN**	**RBFN**
Tibiocalcaneal	81.8	81.0
Tibionavicular	5.9	4.5
Tibiospring 1	9.0	6.9
Tibiospring 2	29.5	22.5
Anterior Tibiotalar	95.6	102.5
Posterior Tibiotalar	124.3	133.3
Talocalcaneal Interosseous	36.3	35.3
Plantar Fascia 1	31.9	32.5
Plantar Fascia 2	47.9	48.7
Plantar Fascia 3	39.9	40.6
Plantar Fascia 4	16.0	16.2
Plantar Fascia 5	159.2	163.8
Spring 1	17.8	16.6
Spring 2	2.5	1.7

Table 3.10: Stiffness Predictions for Post-Op X-Ray Kinematics. Each of the optimal ANNs were supplied with the patient-specific post-operative kinematics. The resulting stiffness predictions are shown above; all were within range of the training data.

	Height (mm)		Angle (degrees)	
	Navicular	**1st Cuneiform**	**Talo-1st Metatarsal**	**Talo-Navicular**
FFN Model	10.91	7.31	19.17	24.72
RBFN Model	10.60	7.09	19.44	25.55
Post-Op Model	10.60	7.18	21.38	24.19
Post-Op Radiograph	14.97	11.18	19.05	25.01

Table 3.11: Post-Operative Kinematic Measures. Kinematics resulting from foot/ankle models utilizing stiffness predictions from the optimal ANNs are listed, as are those kinematics from the pre-operative model [11] and the patient radiograph.

	Percent Difference			
	Height		Angle	
	Navicular	1st Cuneiform	Talo-1st Metatarsal	Talo-Navicular
FFN Model	27.12	34.62	-0.63	1.16
RBFN Model	29.19	36.58	-2.05	-2.16
Post-Op Model	29.19	35.78	-12.23	3.28

Table 3.12: Percent Difference Relative to Post-Op Patient Radiograph. In comparison to the post-operative model, the foot/ankle model using FFN-predicted stiffnesses showed improved performance. Measures were closer to the patient-radiographic kinematics with the most improvement shown among the angles. Angles were also better represented by the computational model using the RBFN-predicted stiffnesses rather than the post-operative model using the originally assigned stiffnesses. (Negative percentages indicate an over-prediction relative to X-ray data.)

3.3 Effect of Ligament Group on Kinematics, Pre-operative Data

Among the datasets generated, those capturing the effects of a single ligament grouping were further analyzed to determine whether any noticeable trends existed between the grouping and a given kinematic measure. Data resulting from stiffness variations referencing attenuated values were analyzed separately from those stemming from variations referencing normal stiffnesses (Figures 3.3-3.14), and p-values were calculated for each set of data (Tables 3.13-3.14). A p-value below $\alpha = 0.05$ indicated that the slope of the trendline was different from zero.

In the case of the talo-1st metatarsal angle, both medial and plantar ligament groupings demonstrated a significant p-value indicating a slope different than zero. Specifically, from Figures 3.3-3.4, it can be seen that T1MT tended to decrease as medial stiffness increased (plantar, spring groups at constant values); the same was true when varying only the plantar grouping (Figures 3.5-3.6). Interestingly, the spring ligament grouping resulted in data depicting no significant trend regardless of varying stiffnesses from normal or attenuated values (Figures 3.7-3.8).

	p-value	
	Stiffness variations from	
Ligament Grouping	**Normal**	**Attenuated**
Medial	p-val <<<0.001*	p-val <<0.05*
Plantar	p-val <<<0.001*	p-val <<<0.001*
Spring	0.480	0.060

Table 3.13: p-values, Talo-1st Metatarsal Angle versus Percent Stiffness Variation. A p-value < 0.05 = α was significant (*) and demonstrated that the slope of the trendline was different from zero. Per the p-values here, only the spring grouping had a negligible effect on T1MT.

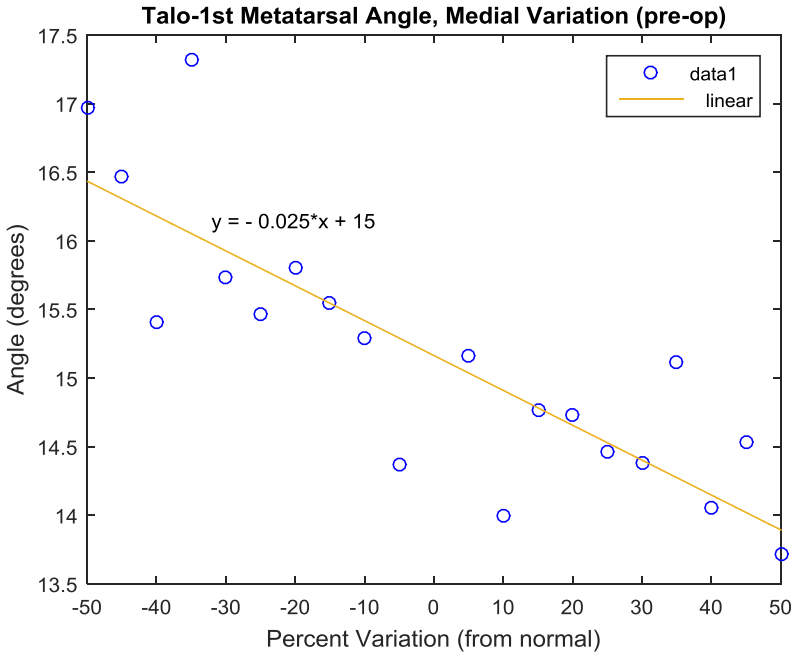

Figure 3.3: Effect of varying stiffness of medial ligament grouping on talo-1st metatarsal angle when varying from normal stiffness values. A significant, decreasing trend in T1MT is observed as stiffness increases.

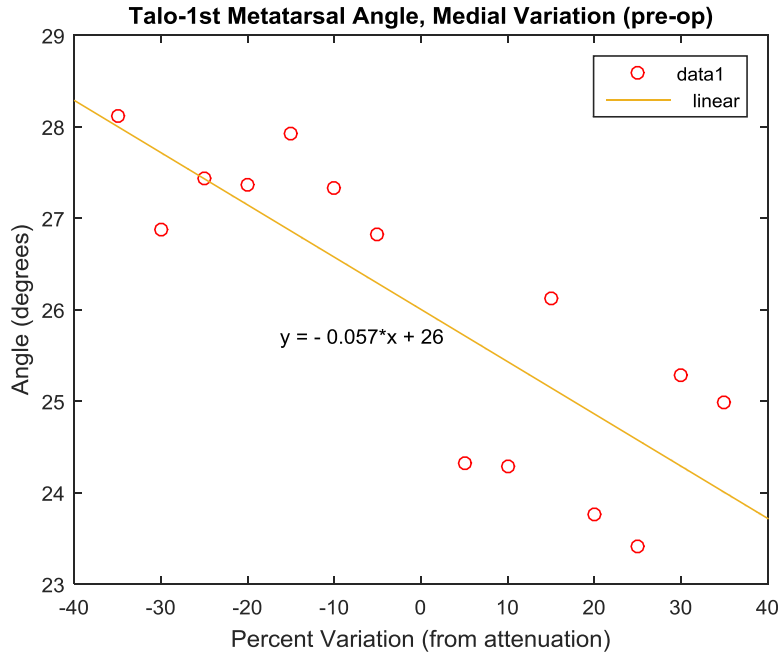

Figure 3.4: Effect of varying stiffness of medial ligament grouping on talo-1st metatarsal angle when varying from attenuated stiffness values. As was the case with varying stiffness from normal values, a decreasing trend was observed between T1MT and stiffnesses adjusted from attenuated values (p-val << 0.05).

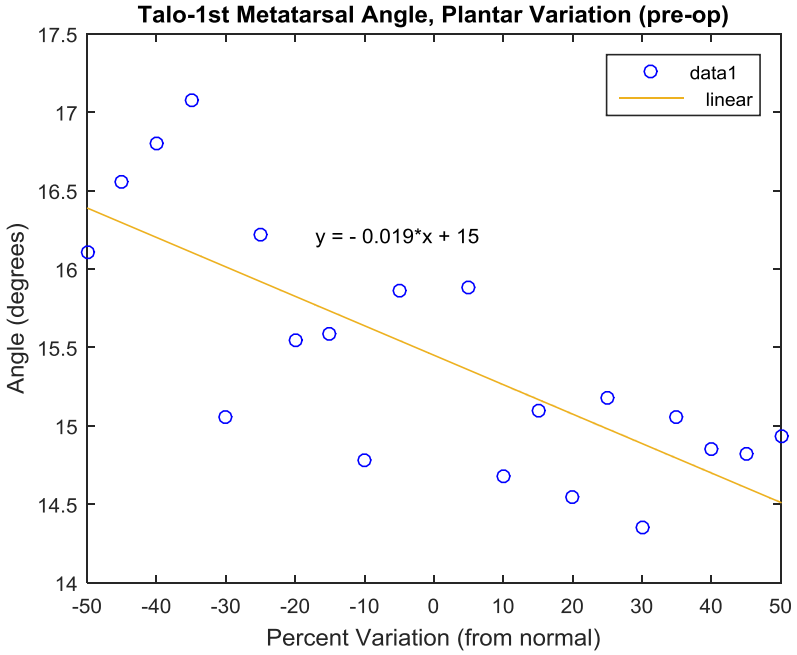

Figure 3.5: Effect of varying stiffness of plantar ligament grouping (from normal stiffnesses) on talo-1st metatarsal angle. Similar to the effects of varying only the medial ligament stiffnesses, a variation of plantar ligaments alone resulted in decreasing T1MT with increasing stiffness (p-val << 0.05).

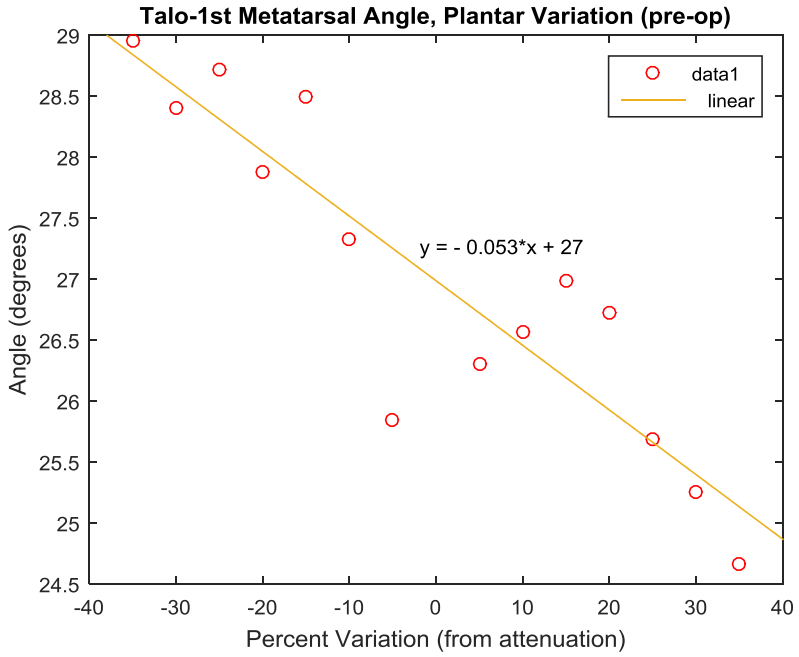

Figure 3.6: Effect of varying stiffness of plantar ligament grouping on talo-1st metatarsal angle when varying from attenuated stiffness values. Angle ranges are higher when varying from attenuated values versus normal stiffnesses; however, the decreasing trend remains common between the two sets of data.

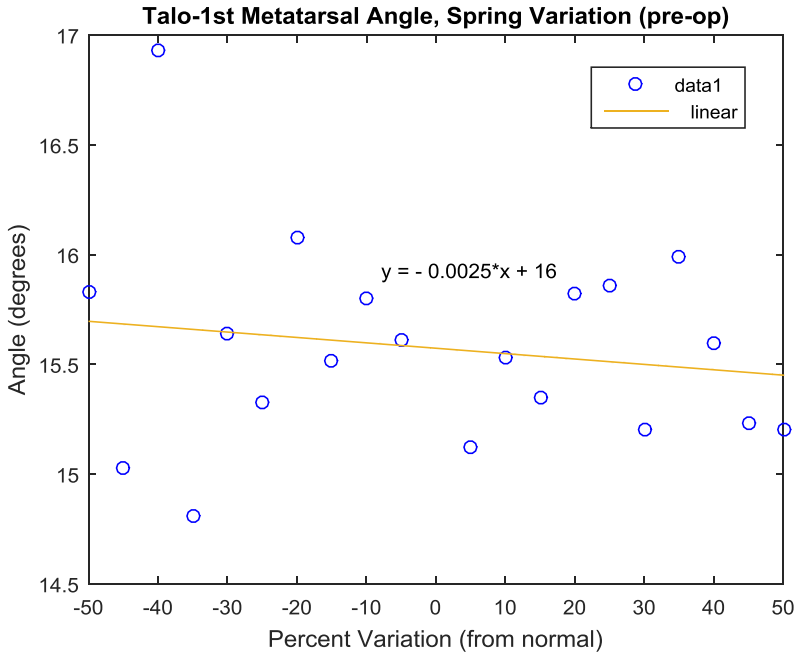

Figure 3.7: Effect of varying stiffness of spring ligament grouping on talo-1st metatarsal angle when varying from normal stiffness values. No noticeable trend was observed between ligament variations and T1MT as the p-value was insignificant.

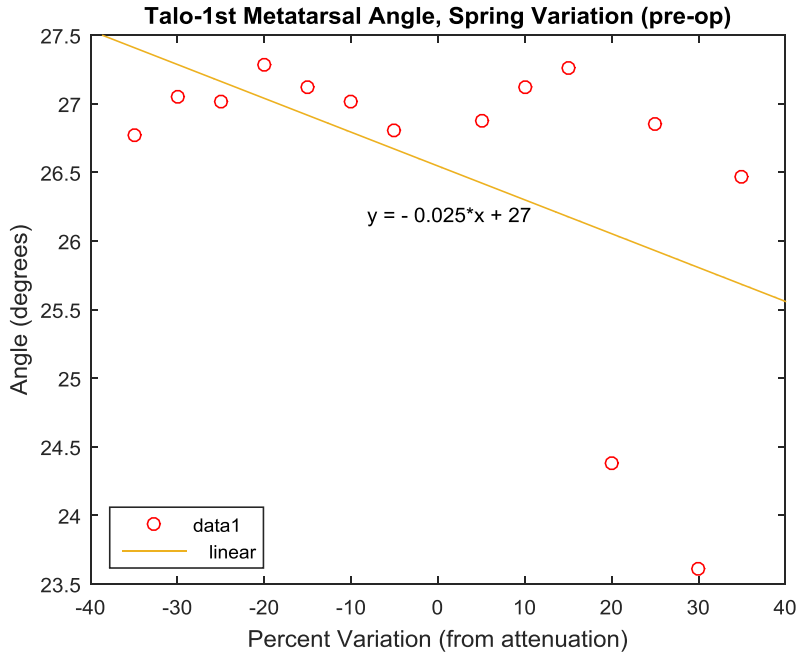

Figure 3.8: Effect of varying stiffness of spring ligament grouping on talo-1st metatarsal angle when varying from attenuated stiffness values. A p-value of approximately 0.12 indicated no significant trend between stiffness variation from attenuation and T1MT.

With regard to talo-navicular angle, three groupings resulted in a significant slope: the medial grouping when stiffnesses were varied from attenuation (Figure 3.10) and the plantar and spring groupings when stiffnesses were varied from normal values (Figures 3.11 and 3.13). The remaining datasets shown among Figures 3.9-3.14 did not illustrate significant changes in slope.

	p-value	
	Stiffness variations from	
Ligament Grouping	**Normal**	**Attenuated**
Medial	0.575	0.001*
Plantar	0.027*	0.461
Spring	0.001*	0.058

Table 3.14: p-values, Talo-Navicular Angle versus Percent Stiffness Variation. A p-value < 0.05 = α was significant and demonstrated an existing trend between TN and changing stiffness. Only those groupings indicated with (*) had significant trends.

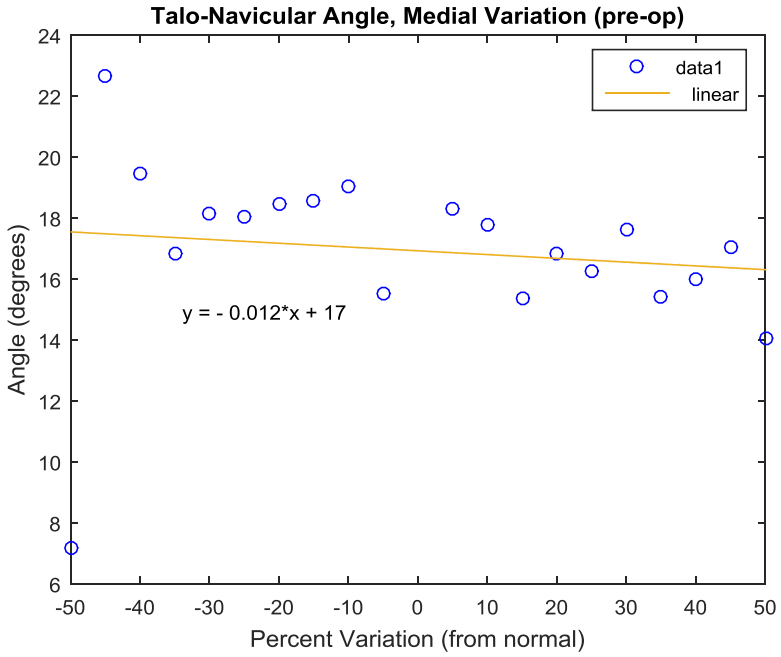

Figure 3.9: Effect of varying stiffness of medial ligament grouping on talo-navicular angle when varying from normal stiffness values. Here, the slope of the trendline was not significantly different than zero.

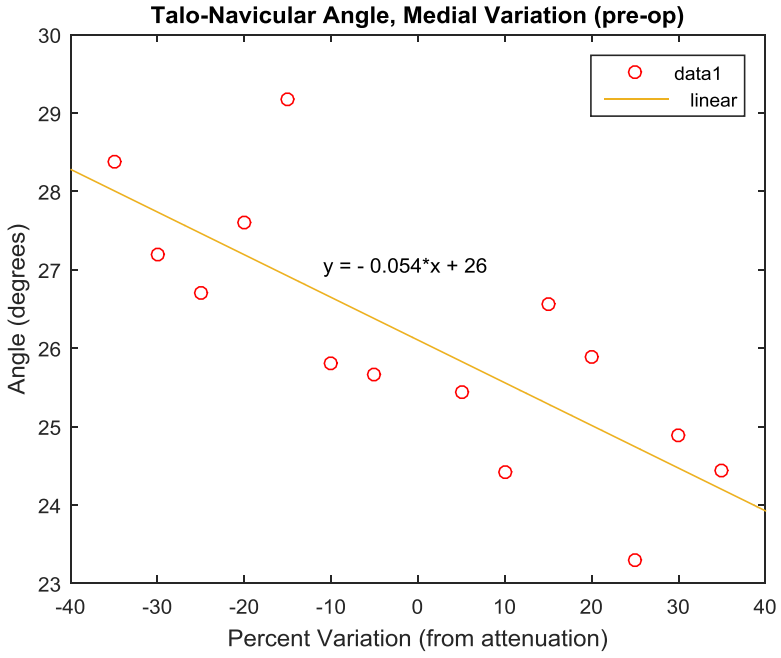

Figure 3.10: Effect of varying stiffness of medial ligament grouping on talo-navicular angle when varying from attenuated stiffness values. As stiffness increased, talo-navicular angle tended to decrease (p-val = 0.001).

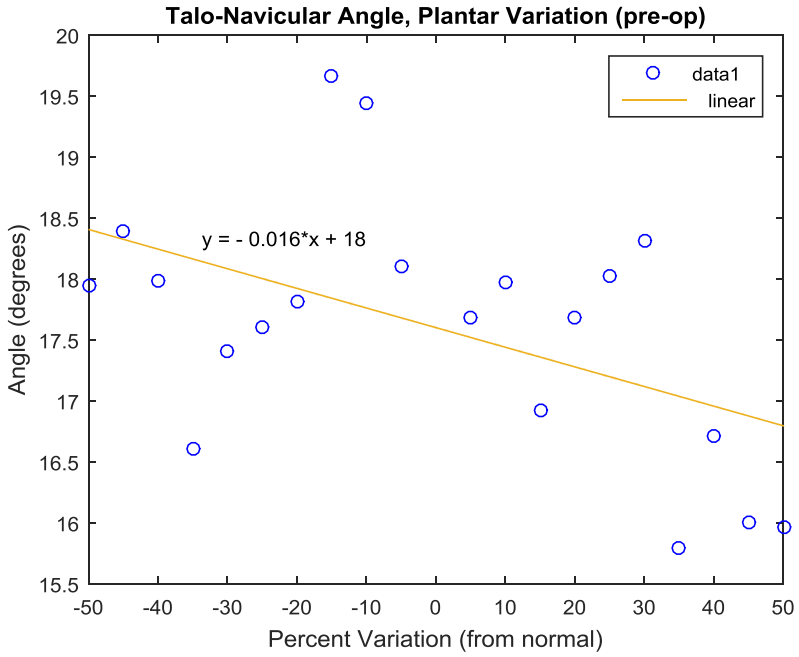

Figure 3.11: Effect of varying stiffness of plantar ligament grouping on talo-navicular angle when varying from normal stiffness values. The slope of the trendline was significantly different than zero (p-val = 0.027).

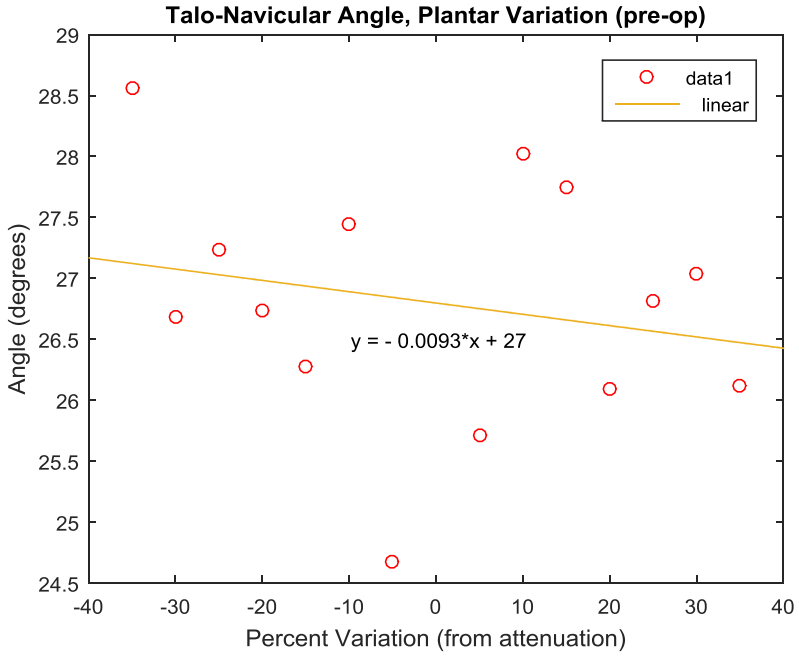

Figure 3.12: Effect of varying stiffness of plantar ligament grouping on talo-navicular angle when varying from attenuated stiffness values. Again, no significance, and thus no trend, was observed.

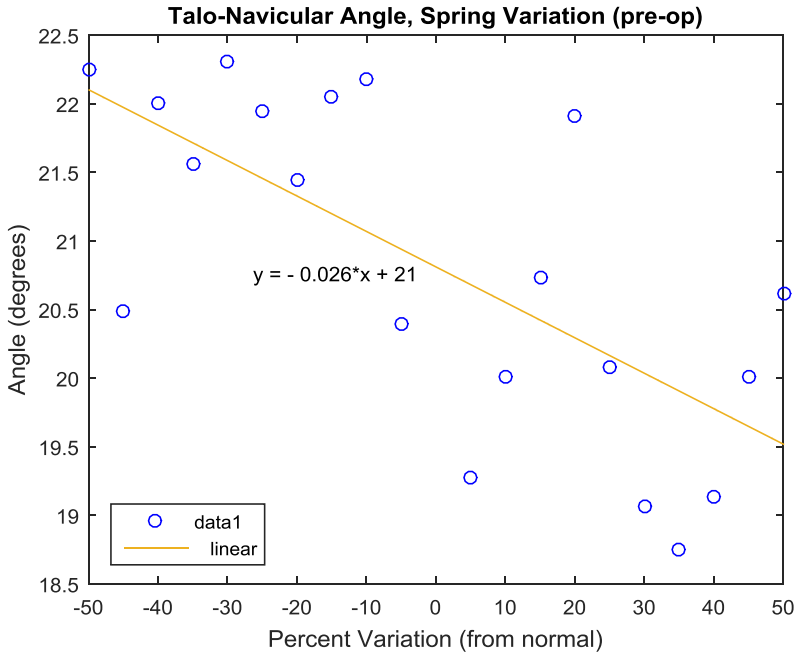

Figure 3.13: Effect of varying stiffness of spring ligament grouping on talo-navicular angle when varying from normal stiffness values. As ligament stiffnesses increased, TN angles decreased (p-val = 0.001).

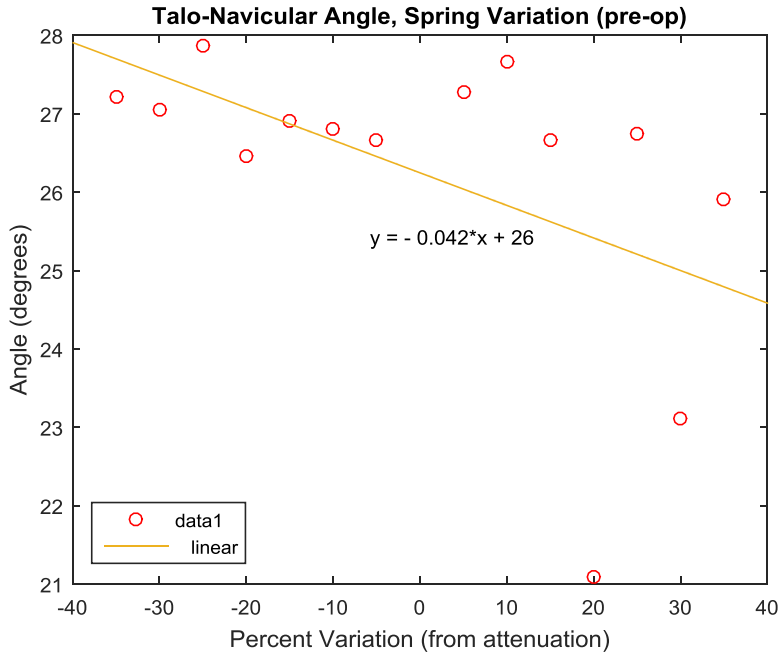

Figure 3.14: Effect of varying stiffness of spring ligament grouping on talo-navicular angle when varying from attenuated stiffness values. No significant trend was apparent among these data (p-val = 0.058).

3.4 Effect of Ligament Group on Kinematics, Post-operative Data

When post-operative data was observed, significant trends were noted among some of the data with the direction of the trend being the primary distinction between these trends and those observed pre-operatively. Upon observing their effects on talo-1st metatarsal angle (Table 3.15), both medial and plantar groupings (whether varied from normal or attenuated stiffness values) showed significant trends with T1MT increasing with increasing stiffness (Figures 3.15-3.18). The spring grouping demonstrated a significant trend when varied from normal while insignificance was noted when spring components were varied from attenuation (Figures 3.19-3.20).

	p-value	
	Stiffness variations from	
Ligament Grouping	**Normal**	**Attenuated**
Medial	p-val <<<0.001*	p-val <<<0.001*
Plantar	p-val <<<0.001*	0.002*
Spring	0.001*	0.458

Table 3.15: p-values, Talo-1st Metatarsal Angle versus Percent Stiffness Variation. A p-value < 0.05 = α was significant (*) and demonstrated a significant trend between T1MT and a given stiffness grouping. Only the spring group, when stiffness was varied from attenuated values, resulted in a negligible effect on T1MT.

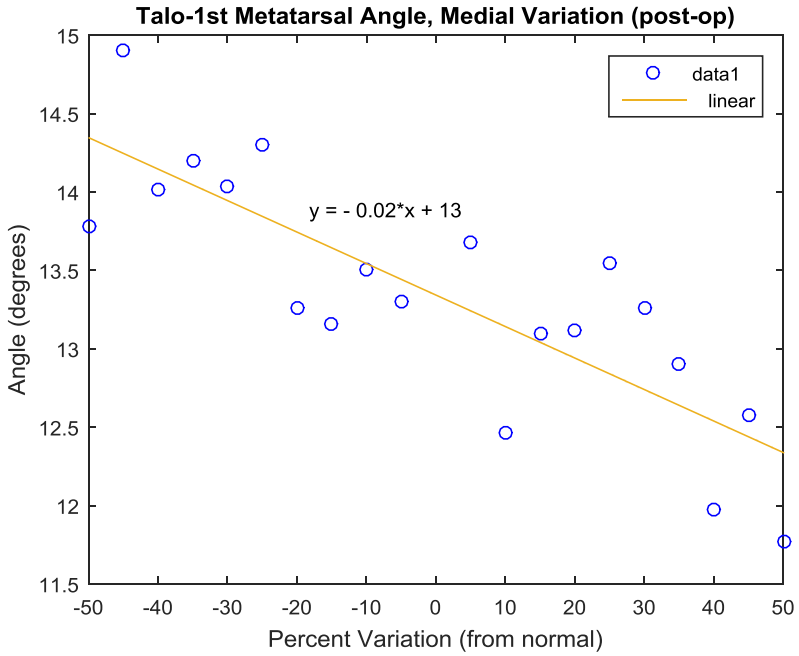

Figure 3.15: Effect of varying stiffness of medial ligament grouping on talo-1st metatarsal angle when varying from normal stiffness values. Post-operatively, T1MT demonstrated a decreasing trend as stiffness increased.

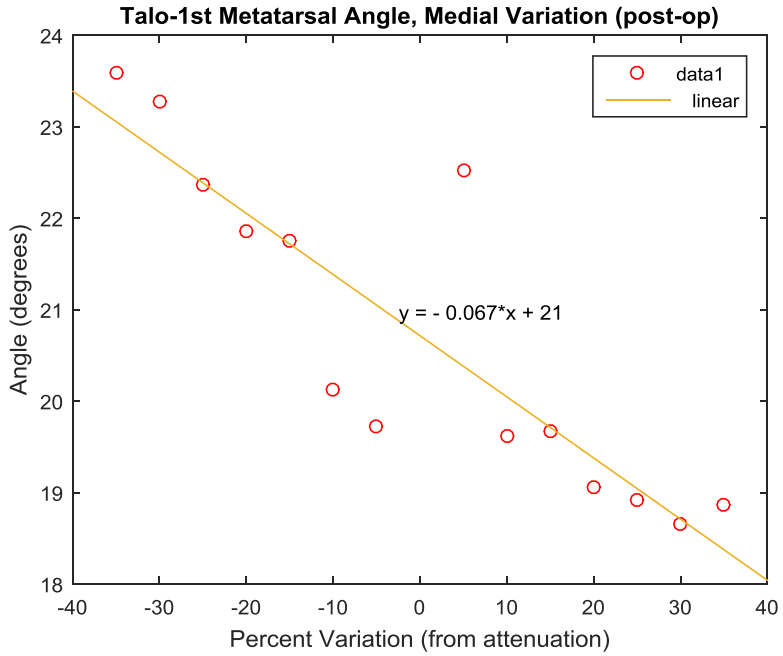

Figure 3.16: Effect of varying stiffness of medial ligament grouping on talo-1st metatarsal angle when varying from attenuated stiffness values. Again, a significant p-value was determined and a negative trend between T1MT and medial ligament stiffness was noted.

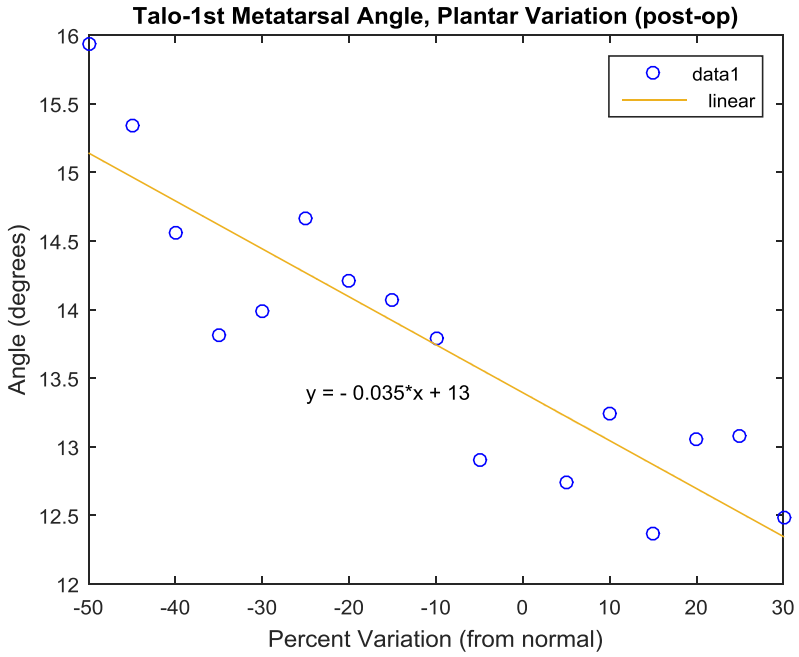

Figure 3.17: Effect of varying stiffness of plantar ligament grouping on talo-1st metatarsal angle when varying from normal stiffness values. Again, a significant p-value was determined and a negative trend between T1MT and ligament stiffness was noted.

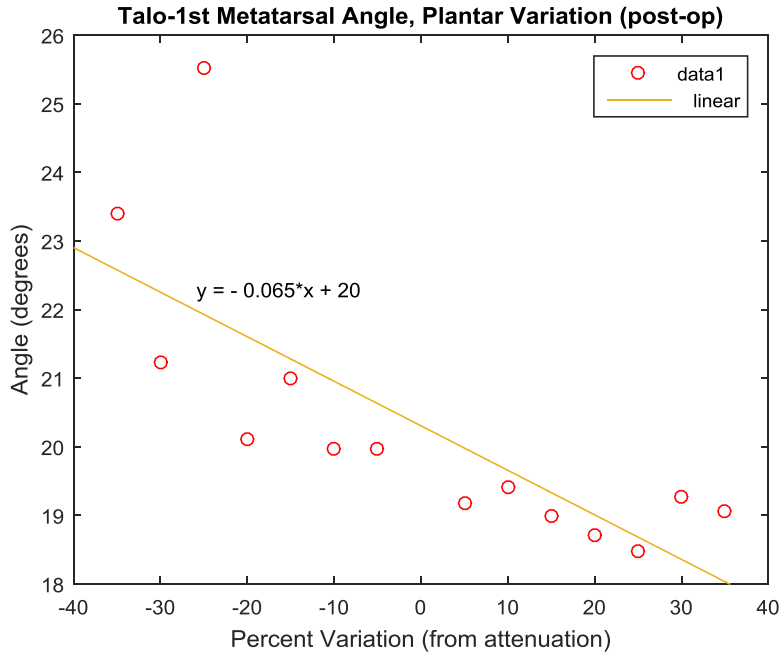

Figure 3.18: Effect of varying stiffness of plantar ligament grouping on talo-1st metatarsal angle when varying from attenuated stiffness values. As with plantar stiffnesses varied from normal, stiffness variations referencing attenuated values also resulted in T1MT angles that decreased with increasing stiffness.

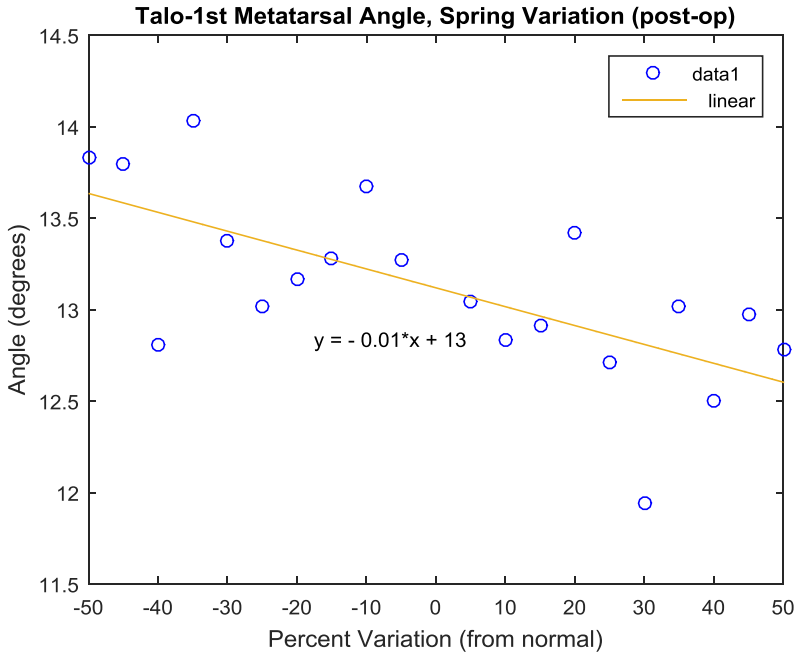

Figure 3.19: Effect of varying stiffness of spring ligament grouping on talo-1st metatarsal angle when varying from normal stiffness values. A significant p-value was determined and a negative trend between T1MT and ligament stiffness was noted.

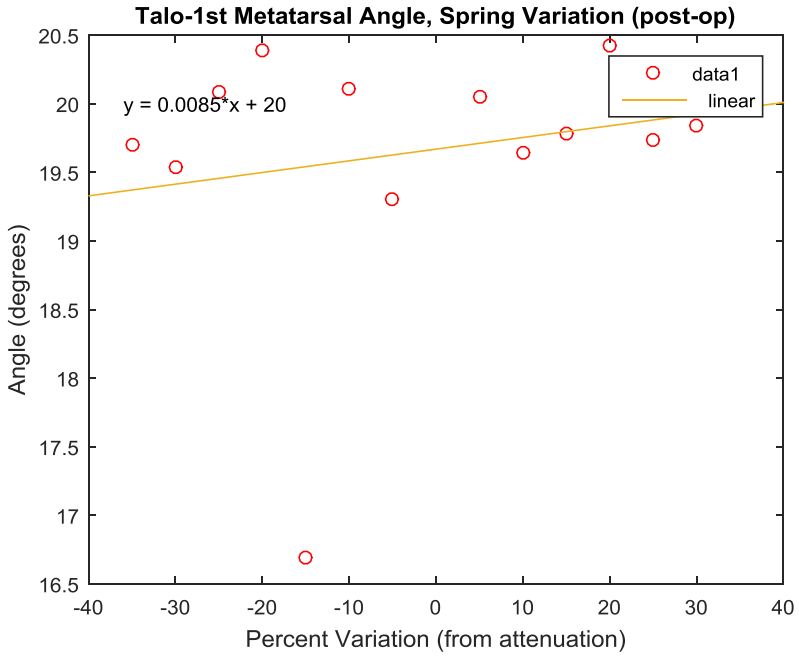

Figure 3.20: Effect of varying stiffness of spring ligament grouping on talo-1st metatarsal angle when varying from attenuated stiffness values. An insignificant p-value was determined thus indicating little to know effect of stiffnesses adjusted from attenuated values on T1MT.

Medial and plantar group variations in stiffness resulted in significant and insignificant trends, respectively, regardless of varying from normal or attenuated values (Figures 3.21-3.24). Variations from normal spring ligament values resulted in a significant trend with talo-navicular angle increasing with increasing stiffness; however, no trend was noted among talo-navicular angles corresponding to stiffness variations adjusted from attenuated values (Figures 3.25-3.26). p-values are shown in Table 3.16.

	p-value	
	Stiffness variations from	
Ligament Grouping	**Normal**	**Attenuated**
Medial	p-val <<0.05*	0.017*
Plantar	0.287	0.366
Spring	0.006*	0.823

Table 3.16: p-values, Talo-Navicular Angle versus Percent Stiffness Variation. A p-value < 0.05 = α was significant (*) and demonstrated that the slope of the trendline was different from zero. When normal stiffnesses were the reference for variation, the medial and spring groups resulted in significant p-values, while only the medial grouping showed a significant trend between TN and stiffness when the latter was varied from attenuated values.

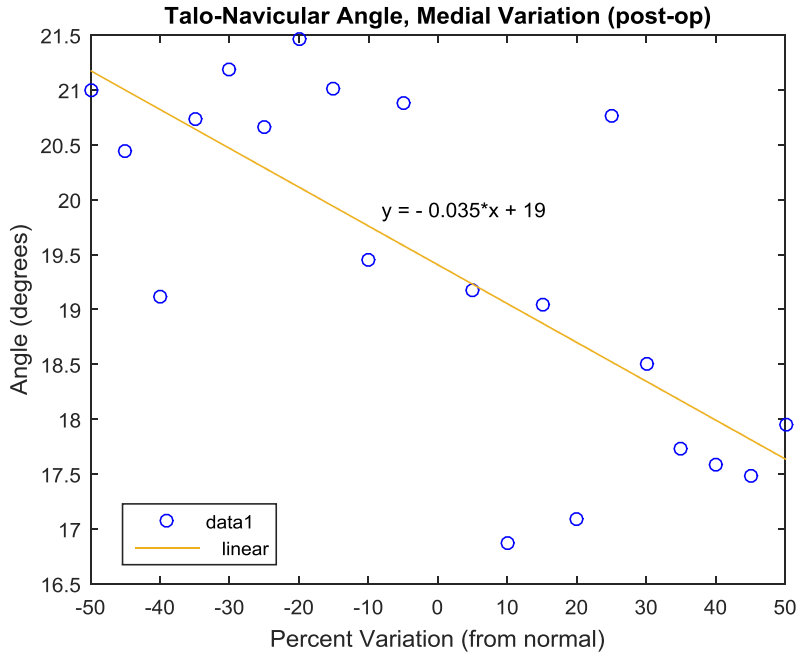

Figure 3.21: Effect of varying stiffness of medial ligament grouping on talo-navicular angle when varying from normal stiffness values. An increasing stiffness of medial ligaments demonstrated a decrease in TN.

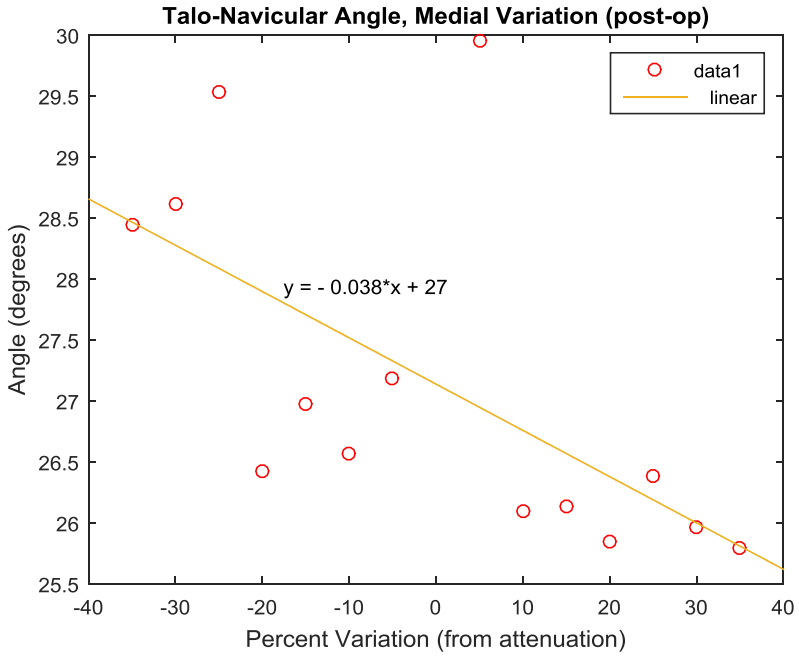

Figure 3.22: Effect of varying stiffness of medial ligament grouping on talo-navicular angle when varying from attenuated stiffness values. A significant p-value was determined thus indicating a decreasing TN with rising stiffness.

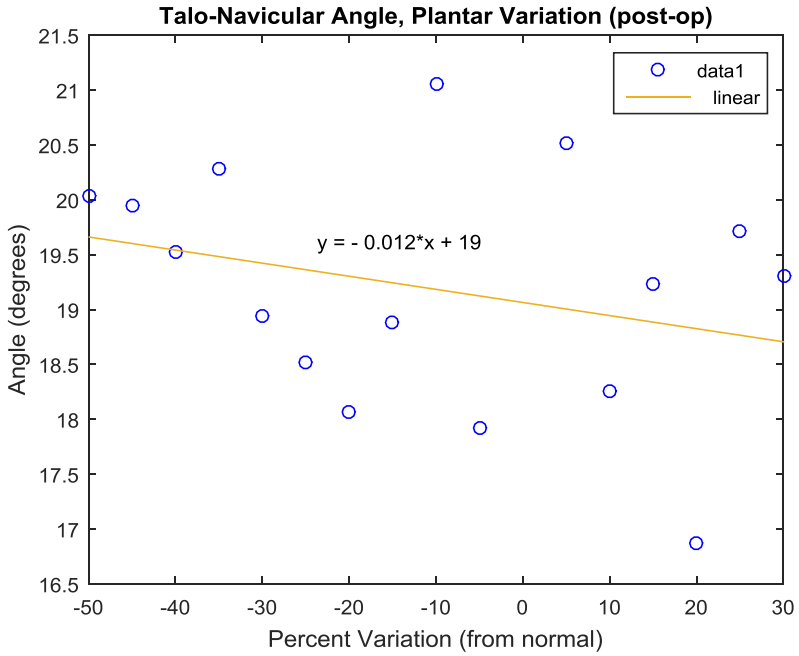

Figure 3.23: Effect of varying stiffness of plantar ligament grouping on talo-navicular angle when varying from normal stiffness values. Changes in plantar ligament values resulted in negligible effects on talo-navicular angle.

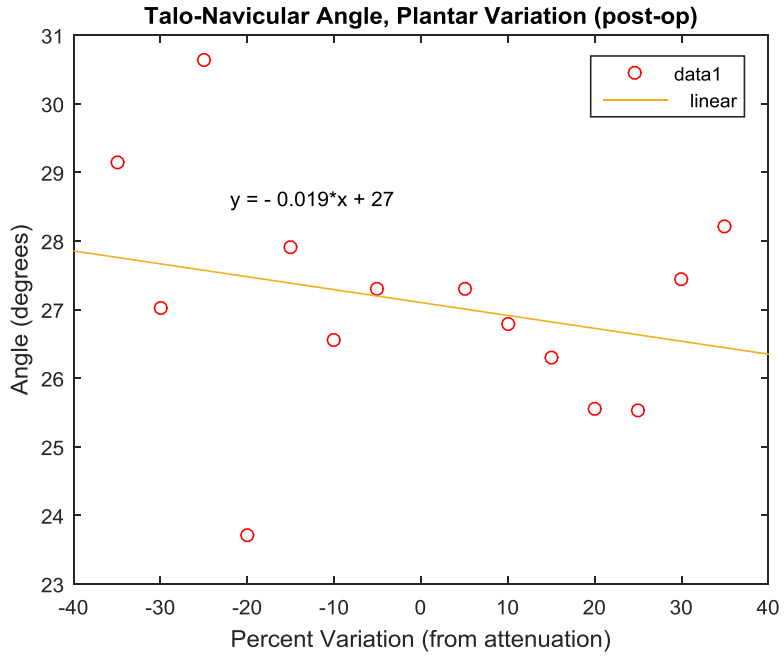

Figure 3.24: Effect of varying stiffness of plantar ligament grouping on talo-navicular angle when varying from attenuated stiffness values. No significant slope, and therefore trend, was revealed between TN and plantar stiffness.

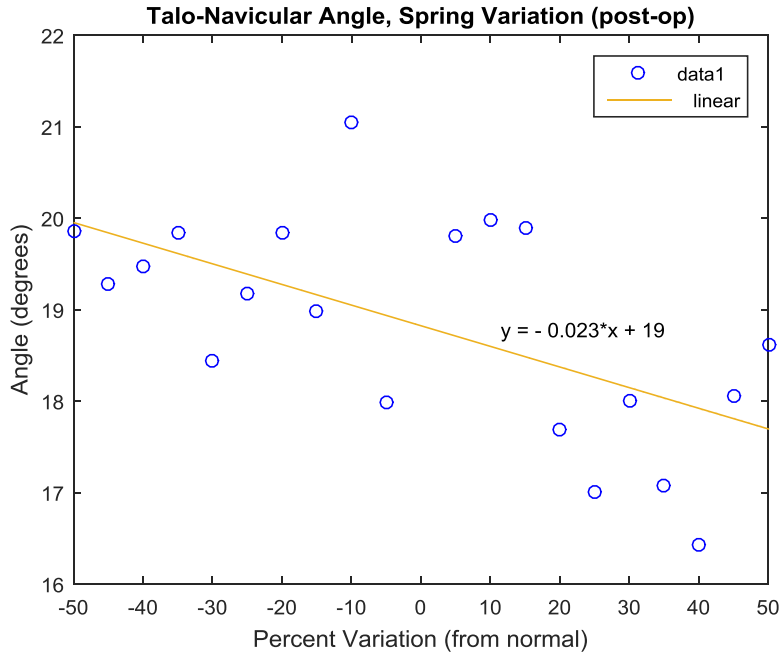

Figure 3.25: Effect of varying stiffness of spring ligament grouping on talo-navicular angle when varying from normal stiffness values. TN was found to decrease with increasing stiffness when variations were adjusted from normal values.

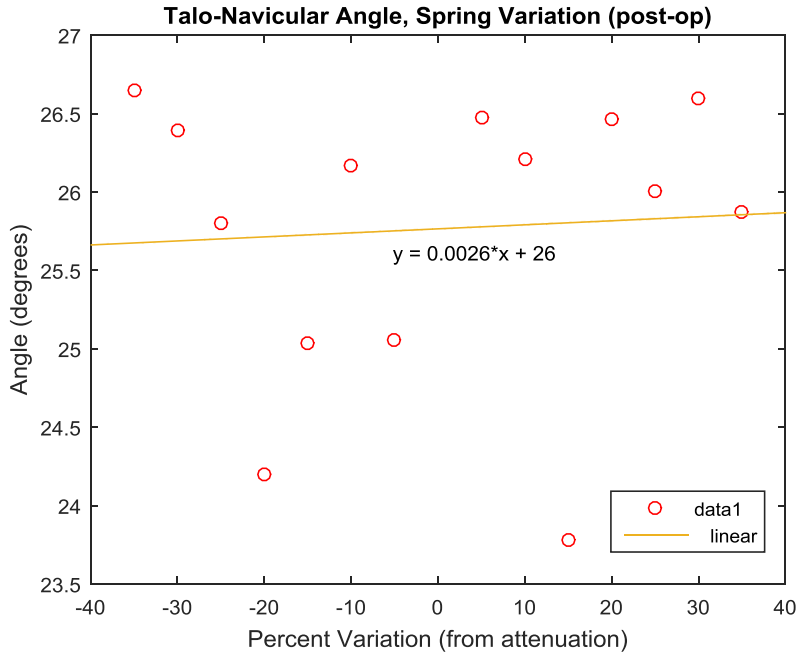

Figure 3.26: Effect of varying stiffness of spring ligament grouping on talo-navicular angle when varying from attenuated stiffness values. Although a significant p-value was calculated between TN and stiffnesses adjusted from normal values, no trend was noted between TN and spring stiffnesses adjusted from attenuated values.

CHAPTER 4 Discussion

4.1 Artificial Neural Network Usage

Artificial neural networks were explored in the current work for several reasons. First, the relationship between ligament stiffness and foot/ankle kinematics is not fully understood, including the effect on kinematics due to the contribution of a single ligament or several in combination. Given that the input-output relationship does not necessarily need to be well understood prior to ANN application [34-35], as is the case in the current work, neural networks were considered a viable methodology to employ. Additionally, it has been shown theoretically that an ANN with a single hidden layer can model any function [34, 45], and so this knowledge was also utilized in the implementation of the single-layered FFN and RBFN.

While a "trial-and-error" type process could have been implemented in the determination of an optimal ligament stiffness set for the foot/ankle computer model, the manual substitution of stiffness values to achieve a certain kinematic measure would have been computationally intensive. Furthermore, as stated previously, because the contributions of individual or groups of ligaments are not currently well-defined, manual determination of stiffnesses would not have necessarily guaranteed that these values

represented the optimal set. Overall, such an approach would have been an impractical, long-term solution. An argument might be made that data gathering for ANN training can also be computationally intensive; however, this computational expense occurs up-front and ultimately the network learns from this data, determines a relationship, and predicts the optimal outputs without further manual manipulation by the researcher. In short, ANNs provided a more efficient and reliable means of finding appropriate ligament stiffnesses in comparison to a trial-and-error method.

In addition to the above, artificial neural networks were used in the current research after reviewing various biomedical examples, including some found in the biomechanical arena [3, 35, 37, 42, 45, 52-54, 60]. Among these investigations, the studies by Lu et al. [3], Eskinazi and Fregly [53], and Kaufman et al. [60] will be highlighted here. ANNs were utilized by Lu et al. to solve for cartilage stress in a computationally modeled knee. Reaction forces due to cartilage contact, produced by a multibody model, represented the inputs to the neural networks, and von Mises stresses determined from a finite element (FE) knee model served as the outputs of the ANNs. The investigation resulted in successful predictions of cartilage stress, which the researchers were able to demonstrate by making comparisons to their ground truth FE model [3].

Like Lu et al., Eskinazi and Fregly also used simulated data to train neural networks for a biomechanical purpose. In this study, contact in a knee implant, represented by a computationally modeled femoral component and tibial plateau, was explored. Inputs and outputs to the neural networks included translations and rotations and contact forces and torques, respectively, that were observed between the modeled knee

components. The trained networks were eventually used to output contact predictions and did so more accurately and faster than the researchers' existing surrogate model [53]. Finally, Kaufman et al. used neural networks to classify different levels of healing after bone fracture. Both intact and fractured bones were represented by a vibrating cylindrical beam, and this beam's behavior was then characterized by an electrical model, specifically its admittance values. These admittance values served as the inputs to the neural networks, while four classifications of fracture healing represented the outputs. Good ANN performance was observed, and as a result, the investigators sought to expand the study to animal and human subjects [60].

Finally, after consulting studies such as those just described, a preliminary study was conducted using a separate patient-specific computational foot/ankle model. As described earlier in Section 1.4.1, this study utilized a smaller set of training data and supplied it to a feedforward neural network; mean square error and correlation data demonstrated good overall performance. Additionally, the network predicted ligament stiffnesses within 5% of the target stiffnesses. Due to the promising results of this preliminary study, as well as the many examples of ANN use in the biomedical field described earlier, the use of artificial neural networks were considered applicable to this research [64].

4.2 Use of Single Patient Foot/Ankle Model for Data Generation

Regarding data generation, all datasets used during training were produced from stiffness variations from a single patient-specific model rather than all of the patient-specific, computational models developed in Spratley's work [11]. As mentioned

previously, it is nearly impossible to determine the exact tissue properties *in vivo* for a given individual and no two individuals have the exact same tissue properties, thus necessitating the use of patient-specific models when studying ailments like AAFD. For the same reasons, better characterization of ligament stiffness for one patient-specific, computational model requires training examples from that model alone in order to learn the appropriate input-output relationship that governs that computer model's behavior. While commonalities (like those soft tissues involved and the corrective procedures applied) may be drawn among the different patient models due to the fact that each patient was afflicted with AAFD, the differing kinematic responses of each patient and their associated computational model both pre- and post-operatively demonstrate how data from one patient model cannot be used to characterize another. As a result, ANN training cannot be conducted with a separate patient's model data.

4.3 Kinematic Ranges, Pre- and Post-Operative

In order to facilitate proper network training, a wide range of scenarios were generated from both the pre- and post-operative foot/ankle models, which is depicted by the range of angles presented in Figures 3.1 and 3.2. The ranges of both the talo-1st metatarsal and talo-navicular angles represented the kinematic outcomes of stiffness variations from both attenuated and normal reference values, and simultaneously represented reasonable inputs for which the neural networks could make predictions. Further, it was sensible to expect that stiffnesses predicted by these networks would fall into ranges corresponding to the stiffnesses that produced the aforementioned kinematic ranges. As mentioned previously, artificial neural networks are suited to interpolation

problems rather than extrapolation [69], and so network responses falling within the limits of the training data indicate one measure of appropriate ANN performance. Per expectation, in this work, the selected optimal networks were provided kinematic data that fell in the range of the training inputs, as did the final stiffness predictions (Tables 3.3-3.4, 3.9-3.10).

4.4 Neural Network Performance, Pre- and Post-Operative

With regard to network selection, performance on the validation set determined the optimal ANN while mean square error on the test set provided a true measure of the network's performance. As training performance tends to be biased (optimistic) because the network is attempting to fit a larger amount of data that also potentially includes noise, a second subset of data must be evaluated to determine true network performance. However, when multiple networks must be compared to one another to find optimal network design, the second set of data contains bias, too, as it is used to evaluate several networks to assess the effects of varying parameters. Therefore, a true representation of the network's performance is obtained on a third (i.e. test) set of data, which is previously unseen by the network [49, 70]. Here, it is important to emphasize that, while a performance value is obtained on the test set, the test set itself does not contribute to network training or parameter adjustment [43]; rather, it provides an idea of the network's ability to generalize, or predict outputs for similar, unseen data [49].

The goal when observing a network’s mean square error is to minimize it (networks’ objective), and here, mean square errors were generally low. When validation set performances were compared in both the pre-operative and post-operative cases, the

FFN had a smaller MSE than the RBFN, though the opposite was true for the test set performances. Performance error was more consistent for the optimal RBFN than FFN as the former's test set error was similar to its validation error. Based on a comparison of validation performances only, the FFN may be favored over the RBFN; however, because their MSEs are similar, it is fair to say that either network would likely provide reasonable stiffness predictions for the pre- and post-operative foot/ankle models.

Finally, to query the network, the entire known dataset was fed to the network utilizing optimized parameters determined during training. These datasets had smaller mean square errors than the validation sets; this was expected given that the number of datasets utilized in the error calculation was much higher than that used in the test subset. Further, both of the optimal networks produced high correlation values between target and predicted stiffnesses ($R = 0.98$) indicating good performance when predicting for the dataset as a whole. The combination of low mean square errors and good correlation on the observed subsets supported the use of these two networks for further stiffness prediction.

4.5 Training Methodologies; Network Sizes

To ensure that the smallest error possible was obtained during training, two tactics were pursued: (1) training a large number of networks with different parameter combinations and (2) using a cross-validation training method. A large number of networks was tested to ensure that an optimal network would be chosen to make future stiffness predictions. Per the literature, higher neuron and hidden layer numbers increase complexity in feedforward networks. This point, along with the previously stated

theoretical rationale, drove the use of a single hidden layer in the FFN. The issue of complexity and the quantity of training data were drivers in the choice of neuron number in that MATLAB's FFN default of ten was used as the maximum network size possible. Furthermore, so as to test various weight parameters, a maximum of ten seed values (0-9) were investigated. By cycling through ten neuron possibilities and ten seed values, multiple network architectures were considered simultaneously, and use of mean square error as the objective function facilitated selection of the optimal choice from those tested. Though the specific neuron selection process differed during RBFN training (due to the means by which RBFNs function), a similar thought process as noted above was utilized for RBFN selection. Because a distance function is used in determining the number of centers, and thus the number of neurons, many more neurons may appear in the hidden layer. Here, 80 centers were cycled through, in addition to the different RNG states, thus once again ensuring a high number of network architectures from which to choose an optimal performer.

Cross-validation was used during training to ensure that all known data examples were represented at least once in the training subset. As mentioned previously, data was divided into training, validation, and test subsets within the cross-validation procedure. This is not a general requirement for neural network training; oftentimes, data is subdivided into these three subsets and a single pass of this known data determines final network choice. Typically, the training subset is the largest and holds a representative range of the possible network outcomes including extremes of the data. However, in the current work, cross-validation was used during training as it was not easily evident as to

which datasets represented the most extreme of the foot/ankle scenarios. The smallest TN angle did not necessarily coincide with the smallest T1MT angle, and further, these values did not necessarily coincide with the smallest of the stiffness values. Therefore, to ensure that the training subset represented all scenarios at least once, cross-validation was employed. Ultimately, the combination of the methodologies described above ensured that many networks of each type were tested and that the best option (i.e. network resulting in the smallest error) was selected.

With regard to hidden neuron size for each of the optimal networks, whether the pre-or post-operative case, the radial basis function networks resulted in higher neurons. This is unsurprising given the difference in the way the two network types function. While a maximum of ten hidden neurons was implemented during FFN training, the RBFN was not limited to this number. This directly relates to network functionality. RBFNs utilize centers and compare inputs to these centers via a distance calculation and ultimately place Gaussian functions at each of these centers. (Here, the FFN code is cycling through number of neurons while the RBFN code is cycling through number of centers.) Effectively, this means that RBFNs are surveying more finite regions of the input space in comparison to feedforward networks, which are essentially surveying the entirety of the input space. As a result, while it is possible to obtain a larger FFN than RBFN, it is reasonable and not uncommon to expect more neurons in the radial basis function than the feedforward network [43].

4.6 Ligament Stiffness Predictions

4.6.1 ANN-Predicted Stiffnesses versus Assigned Foot/Ankle Model Stiffnesses

After network performance was analyzed to choose the optimal networks, these ANNs were used to make predictions on two specific datasets of interest. First, the kinematic data belonging to the pre- and post-operative foot/ankle models of [11] were presented to their respective optimal networks and used to predict the corresponding stiffnesses. The rationale here was that because these datasets provided the foundation for training data generation, the chosen networks should be able to predict stiffness values similar to those assigned in [11]. For the pre-operative networks (Table 3.3), percent differences between the originally assigned stiffness values (i.e. targets) and those predicted by each of the networks fell at or below approximately 6% (FFN) and 12% (RBFN). For the latter, while 12% represented the maximum difference, only three of 14 ligament components displayed this difference with the remainder of the components differing by percentages more comparable to those produced by the FFN. Overall, however, performances of both networks were considered acceptable and confirmed the aforementioned rationale.

In comparison to the pre-operative networks' predictions, the post-operative networks displayed greater differences between the target stiffnesses of the foot/ankle model and the ANN predictions (Table 3.9) with maximum differences for the FFN and RBFN standing at approximately 18% and 19%, respectively. The larger differences here may be attributed to the differing kinematics (in comparison to the pre-operative

kinematics). Because stiffness values assigned to the post-operative model were the same as those assigned to the pre-operative models, the stiffness variations created from the post-operative model laid within the same set of stiffnesses utilized in network training for the pre-operative model. However, the resulting post-operative kinematics and their respective ranges were similar to, but not identical to those seen pre-operatively (differing trends will be discussed later in Sections 4.3 and 4.4), a phenomenon most likely due to the inclusion of the surgical corrections (tendon transfer and medializing calcaneal osteotomy). Again, the purposes of these surgical corrections are to adjust the arch and hindfoot alignment, thereby effecting an increase in arch height and offloading the medial foot. Therefore, at least some change in kinematics would be expected. This difference in kinematics is relevant given the method by which centers are chosen. Recalling that the series of *for* loops cycles through number of centers in the case of the RBFN, the values of the centers themselves are dependent on the k^{th} number among the training data. Therefore, while both pre- and post-operative training resulted in an optimal k of 10, every tenth value among the pre- and post-operative training inputs were not identical. Although kinematic ranges and hidden neuron numbers were similar pre- and post-operatively, the differences between the two groups may have placed centers at locations that resulted in the noticeable difference observed among pre- and post-operative ligament stiffness predictions seen in Tables 3.3 and 3.9. Nonetheless, each round of training resulted in a single, optimal network among those tested and the kinematic-stiffness pairings used in the current work did result in acceptable network performance. Therefore, one may still

conclude that neural networks provide an adequate means of refining stiffness inputs for the foot/ankle model.

4.6.2 Link between Insignificant Trends and ANN-Predicted Stiffnesses

While trends and their significance will be discussed more fully later in Section 4.8, an interesting note may be made here about insignificant trends and the stiffnesses discussed in Section 4.6.1. Pre-operatively, it was found that all three ligament groupings, whether across a portion of or the entire range of stiffnesses, was found to be insignificant with respect to one or both of the angular measures. For both FFN and RBFN predicted stiffnesses, all or a majority of those components with the highest percent differences relative to the assigned stiffnesses belonged to the groupings found to have an insignificant effect on angular kinematics. In the post-operative case, the plantar and spring groups (again, whether across a part of the stiffness range or its entirety) resulted in insignificant trends among the angular data. Once again, the highest percent differences among ANN-predicted stiffnesses relative to the assigned values predominantly existed in the components comprising ligament groups having negligible effects on kinematics. This data supports further investigation into the role of/interplay between ligament groups and the individual components contained within them.

4.6.3 ANN-Predicted Stiffnesses for Patient Radiographic Data

The networks discussed above were ultimately used to find optimized stiffnesses for the foot/ankle model that would result in kinematics more reflective of patient radiograph. Therefore, the radiographic kinematics were supplied to the optimal networks such that corresponding stiffnesses would be predicted. Given that these kinematics fell

within range of the training data inputs, it was reasonable to consider these radiographic kinematics as a plausible foot/ankle model scenario for which the optimized networks could predict stiffnesses. In relation to the X-ray data, the existing patient model over-predicted the angles and under-predicted the heights of interest. Per [22], flatfooted patients tend to have lower arch heights and larger joint angles than the normal population. Also, it can be practically assumed that relatively stiffer ligaments would improve arch height and decrease joint angles; therefore, new predictions were generally expected to be higher than stiffnesses assigned to the foot/ankle model of [11]. This was true of the fourteen stiffnesses predicted by the FFN and a majority of the component values predicted by the RBFN.

It was also noted that the post-operative stiffnesses predicted by both networks were consistently lower than their pre-operative counterparts. This may be attributed to a combination of the surgical corrections included in the post-operative model and the differences exhibited between the pre- and post-operative kinematic data. Based on the kinematic outcomes of the foot/ankle model in [11], a smaller percent difference between patient model and radiograph was observed post-operatively. The difference in the pre- and post-operative models of [11] is the presence of the FHL transfer and the MCO. In other words, with no change of stiffness, the surgical corrections were able to effect a positive change within the models when the two were compared to the radiographs. Here, the combination of a change in stiffness (due to the use of ANN-predictions in the post-operative models) and the presence of the surgical corrections potentially obscures the degree of individual contribution. In other words, the presence of the FHL transfer and the

MCO may have influenced the effect of stiffness post-operatively. While this may explain the lower stiffness predictions post-operatively, the rationale does not diminish the fact that the ligament stiffnesses do impact the resulting kinematics; and therefore, the use of the ANNs to predict stiffnesses is still valid.

Additionally, it may be noted in Figures 3.1 and 3.2 that the sorted kinematic data take on slightly different shapes pre- and post-operatively. Interestingly, unlike the T1MT values, the pre-operative TN data illustrated a somewhat linear shape when the data was sorted and plotted, with some portions of the data overlapping with T1MT values. Post-operatively, the sorted angular data resembled one another in shape and did not demonstrate any overlaps. Such distinctions may have contributed to differences in ANN predictions between the two sets of training data. A possible future study in which this notion could be tested would involve running the same type of experiment as demonstrated in this work on a second (or more) patient's foot/ankle models. After generating datasets from each individual model and training networks in the manner described in Chapter 2, it would be interesting to see if similar trends in predictions would hold across multiple patients. This may also shed light regarding the aforementioned commentary about the level of influence of surgical corrections versus ANN-predicted stiffnesses. Overall, in the current work, while differences in kinematics were present, the resulting stiffness predictions made by all four networks all fell within ranges of the training data and were considered acceptable for use in the foot/ankle models.

4.7 Foot/Ankle Model Performance using ANN-Predicted Stiffnesses

Following application of the new ligament stiffnesses above, improvement was noted in the pre-operative computational model's performance. As evidenced by the percent differences in Table 3.6, both sets of network predictions generated an improvement in three of the four measures of interest in that they were closer to the radiographic data than those resulting from the assigned stiffnesses in [11]. The FFN performed slightly better than the RBFN with regard to heights, while the reverse was true for the angles. These observations may be tied back to the role of the different ligaments in flatfoot. Because the deltoid components act as the primary restraint on the medial side of the ankle, thus preventing extreme eversion the foot, it may be concluded that slack or relatively less stiff deltoid components could result in more foot eversion and subsequently a lower arch. Recalling that the RBFN resulted in a few components, specifically portions of the medial (deltoid) grouping, that were below the original model assignments, it made sense that the arch heights were lower in the case of the model using RBFN predictions than the case using FFN predictions. Despite the lower deltoid predictions, however, the RBFN's stiffness predictions of plantar components were higher than the assigned values in [11], and likely, the combined effect of the medial and plantar groupings still created better foot/ankle model performance with regard to the heights.

Talo-1st metatarsal angle also improved pre-operatively using both networks' predictions, but here, the RBFN's stiffnesses had a slightly better effect on model performance (i.e. smaller percent difference) than the FFN's predictions. As for talo-navicular angle, the network predictions worsened the resulting measure with the FFN

resulting in a slightly worse prediction than the RBFN, although the angles resulting from both sets of predictions still fell within range of the training data. These results point to an interesting, and possibly new future direction for this research. The specific contributions of a given ligament to AAFD are not well understood, however, the above results suggest that each ligament grouping has a varying effect on the different kinematics. In other words, an equal percent variation in stiffness across all groupings does not equate to the same amount—or even direction—of change in kinematics. Therefore, future iterations of this study could investigate the different groupings individually or even perhaps on a component-by-component basis such that the specific effects of a soft tissue are better understood. This would be accomplished by generating more datasets either at finer percent variations and/or datasets containing combinations of variations on both the grouping and individual component level. Finer increments may elucidate more about the different ligaments' roles on TN angle, for example, given that the TN angle of the existing model already closely predicted that of the radiograph. Varying components individually may indicate the relative stiffness changes necessary to yield the higher arch heights while still maintaining the sought-after angles. Ultimately, although one angle improved but the other did not, the overall results indicate that ANNs are still a viable and valuable mean of honing in on stiffness values for the foot/ankle computer model. Therefore, it may be concluded that added training data would further optimize computational model performance.

Just as with the pre-operative networks, post-operative X-ray kinematics were supplied to the FFN and RBFN to predict corresponding stiffnesses. Of the four measures

of interest, the two heights and one angle were under and over-predicted, respectively, by the existing foot/ankle model, and so, generally stiffer predictions were expected for the medial and plantar groups. The forth measure, talo-navicular angle, was under-predicted by the existing computer model; therefore, less stiff spring ligaments were expected. When compared to the assigned post-operative stiffnesses, the optimal FFN predicted higher stiffnesses for all ligaments, while the RBFN predicted higher stiffnesses for all components except the tibionavicular, tibiospring, and spring components. All predictions, however, were within training data ranges, as were their resulting kinematics.

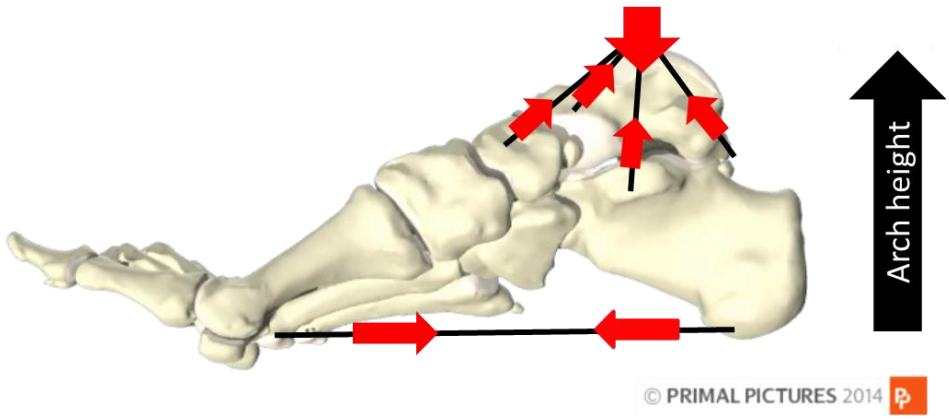

Figure 4.1: Ligamentous support of medial longitudinal arch (right foot), medial view. Tracks of the deltoid (vertical, angled black lines) and plantar (horizontal black line) ligaments are approximated above with red arrows indicating tension in the soft tissues. The resulting effect of stiffer ligaments is an overall increase in arch height. [Adapted from: Primal Pictures for Anatomy TV.]

Performance of the foot/ankle model using the FFN's stiffness predictions demonstrated improvement over the original post-operative model; percent differences among measures relative to the radiograph were smaller. As for the RBFN, navicular height remained consistent and 1st cuneiform height was under-predicted in comparison to the foot/ankle model developed previously. Both angles were improved upon, thus were

closer to the radiographic measurements. In the former case, the improvement of all measures can again be tied back to the role of the different ligaments. When looking at the medial view (Figure 4.1), stiffer medial ligaments pull up the arch while stiffer plantar ligaments effectively make the foot tauter as the anterior and posterior plantar surfaces of the foot move closer to one another. The overall effect is to create a higher arch. Additionally, improved T1MT and TN angles are explained by the supportive role that the spring components have on the talo-navicular joint. In essence, these components prevent collapse or sagging of this joint (appears as an anterior talar tilt in the medial view and an "opening" of the joint in the oblique anterior-posterior view, Figure 4.2); therefore, the relative stiffness of these components would improve or worsen this effect. Here, stiffer ligaments predicted by the FFN illustrated improvement. In fact, the TN angle was closer to the radiographic value but over-corrected. This may suggest that the components involved in talo-navicular joint support may be stiffer than those initially assigned but not as stiff as the predictions made here. The finer stiffness variations and increased number of training datasets mentioned earlier could also lead to further exploration of this idea. Nonetheless, the optimal network discovered among those networks queried in this study still provided enhanced foot/ankle model performance; thereby supporting the use of ANNs for the study objective.

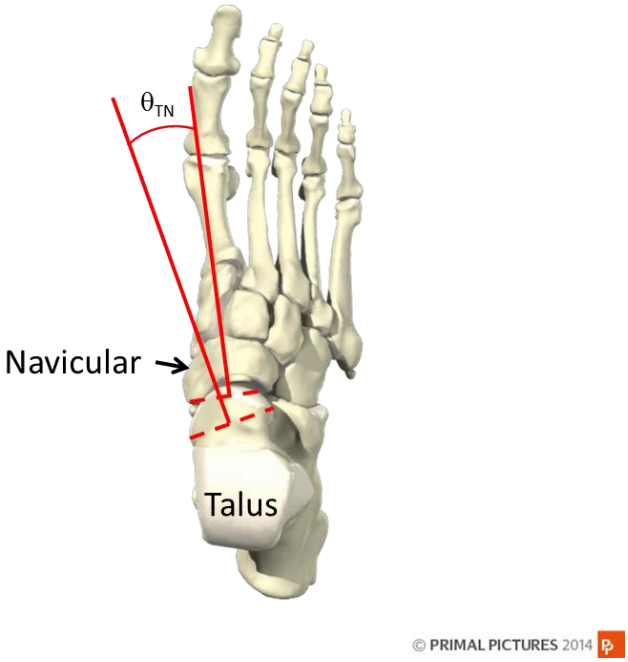

Figure 4.2: Talo-navicular angle (right foot), oblique antero-posterior view. A relatively larger θ_{TN} angle indicates an opening of the talo-navicular joint and is characteristic of a flatfoot. [Adapted from: Primal Pictures for Anatomy TV.]

As for the RBFN, the lesser impact on the heights of the foot/ankle model made sense in light of the less stiff deltoid and spring components. They also helped to explain the slight over-prediction of the radiographic angles in comparison to the model developed by Spratley [11]. Per the explanation provided earlier, less stiff spring ligaments create more laxity in the talo-navicular joint support manifesting as larger angles. However, as a reminder, it must be noted that this over-prediction still represented an improvement of foot/ankle model performance as the percent differences of both these angles relative to the X-ray data were smaller than those resulting from the original post-operative model. Such result draws attention back to a point made previously: the specifics of ligaments' effects, or individual components' effects, on given kinematics remain unclear. In particular, it is

possible that some combination of relatively stiffer plantar components and less stiff spring ligaments generated an overall improvement in foot/ankle model performance despite the over-prediction, though the exact effect of the separate elements is unknown and would require further study.

One additional comment may be made regarding the ligaments. The gap in kinematics between the computer models and the X-ray data may be attributed to the fact that the exact starting values of the patient's ligament stiffnesses were unknown. Again, it is impossible to measure such *in vivo* data; therefore, the originally assigned ligament values were taken from literature. Also, the post-operative model in [11] was assigned the same stiffness values as the pre-operative model and so any healing of ligaments *in vivo* was not modeled. Although this uncertainty may be one source of the difference in computational kinematic prediction and those data measured on the X-ray, the use of literature data was an appropriate, standard means of providing the foot/ankle models with inputs. Additionally, network predictions did result in improvements in computational model performance; thus, the insight garnered here was useful in providing potential future directions for this research such that a better understanding of ligament properties may be ascertained.

4.8 Relationship between Kinematic Measures and Ligament Groupings

Some discussion has already been put forth about the role of specific ligaments in AAFD. As was initially explained, certain ligaments are implicated in the disease process, but the individual contributions of the soft tissues are not well understood. Given that this study examined the computational models of only a single patient, it alone cannot confirm

the exact role of a specific ligament or a grouping of ligaments; however, some interesting notes can be made about the data gathered and may point to areas of future exploration. The kinematic data measured due to variation of only a single ligament grouping, whether from normal or attenuated values, was examined to determine whether the variation in that grouping did in fact affect the measure. Data obtained from normal variations were analyzed separately from those obtained from attenuated variations so as to determine if a significant trend existed within a specific range of stiffnesses. When the talo-1st metatarsal angle was studied in the pre-operative case, both the medial and plantar groups were found to have significant p-values indicating that a variation in stiffness did affect the measure taken. However, T1MT was not found to change significantly when only the spring group was varied. In all instances described, significance or lack thereof was found to be true irrespective of whether the stiffness variation was relative to normal or attenuated values. This suggests that medial and plantar ligaments may be further investigated with respect to T1MT. Specifically, stiffer medial and plantar components could produce smaller T1MT angles (as per the decreasing trend noted in Figures 3.3-3.4), and vice versa, in the flatfooted patient. This makes sense per the literature as relatively larger angles are associated with flatfoot while smaller angles are characteristic of normal feet [22].

Additionally, for both medial and plantar groupings, the decreasing trend between T1MT and stiffness variation was sharper when the latter was relative to attenuation. As was stated earlier, the exact starting values of the patient's ligament stiffnesses were unknown; however, the sharper decline in the attenuated case intimates that relatively less stiff or compromised ligaments have a more drastic effect on the decline of the T1MT

angle. It would be interesting to determine whether this finding were true of the overall progression of the patient's condition; and to do so would require additional data for a patient of interest and/or more patient models. A second level of investigation could also involve component variations. With initial data pointing to the medial and plantar groups of ligaments, the individual elements belonging to these groups could be varied to find out if a particular component affected a particular kinematic more or less than its counterparts.

As for the talo-navicular angle, both plantar and spring groups demonstrated significant trends, but only when varied from normal stiffnesses; the medial grouping displayed a significant decreasing trend when varied from attenuation. These findings imply that all ligament groupings have an effect on talo-navicular angle, but only in specific ranges. Another implication of these results is that, at some point, ligaments may be too compromised to play much of a role in the outcome of the TN measure. This refers particularly to the plantar and spring groupings, further suggesting that the medial group may come into play only when the other groupings are already compromised.

Post-operatively, only the spring group when varied from attenuation did not have a significant impact on talo-1st metatarsal angle; all other groups displayed significant trends between T1MT and percent variation. The significance of the relationships between medial and plantar groups and T1MT is unsurprising as these ligaments' functions effectively pull on the arch of the foot. Unlike in the pre-operative situation, here the spring group adjusted from normal now plays a role in affecting a change in T1MT. Additionally, post-operative data exhibited significant, decreasing trends similar to those observed for the pre-operative data. Because adjustments in stiffness were made

identically in both the pre- and post-operative models, the most likely cause for the difference in the data and trends mentioned above was the inclusion of the surgical corrections in the post-operative foot/ankle model.

Like T1MT, talo-navicular angle also demonstrated decreasing trends where significant in the post-operative model. Significant trends were found among the medial grouping (when adjusted from normal and attenuated values) and the spring grouping when adjusted from normal. Notably, no significance was discovered among the plantar groupings; however, this makes sense when MCO function is considered. This procedure is meant to shift the posterior calcaneus medially to correct for hindfoot valgus, which is commonly identified as "too many toes." In AAFD, a flattened arch and opening of the talo-navicular joint causes the forefoot to move laterally and the hindfoot to abduct, and so, medializing the heel of the foot brings it back into alignment thus correcting for the over-abduction. Essentially, this also corrects the position of the navicular relative to the talus, thereby closing the talo-navicular angle. Therefore, the effect of plantar ligaments with respect to the TN angle may have been deemed negligible due to the corrective influence of the bony surgical procedure.

Similarly, the medial groupings' impact on the TN angle may have been assisted by surgical corrections. In addition to the MCO, a tendon transfer was also implemented, the purpose of which is to add soft tissue support to the medial longitudinal arch. With assistance in pulling up the arch, perhaps the medial ligaments are better able to support the arch across a wider range of stiffnesses, subsequently reducing the abduction and eversion of the foot and closing the TN angle.

In summary, changes in the significance of linear fits pre- and post-operatively were likely due to the surgical interventions implemented. The pre- and post- models were assigned the same starting stiffness values from which ANN training data was generated; and thus, the only major difference between the two that could affect the influence of stiffness on kinematic changes, and by extension significant trends, were the FHL transfer and MCO. As stated earlier, some combined effect of stiffness and surgical correction was at play in the post-operative model, thereby possibly enhancing or diminishing the relative contributions of different ligament groupings. (Note: The assigned stiffnesses were the same because no post-operative MRI was taken at the time of patient follow-up [11]. Thus, any possible soft tissue remodeling was not accounted for in the patient model. Whether such MRI was taken, however, the exact stiffness values would still be unknown pre- and post-operatively due to the inability to capture this data *in vivo.* Therefore, the use of identical stiffnesses in both pre- and post-operative foot/ankle models was reasonable.)

Additionally, as is illustrated by all of the above results, some amount of interdependency among the different ligaments exists, and this warrants further investigation into the effects of the groupings on the kinematics of the foot/ankle. This finding also hints at the need to investigate the independent role, as well as the interdependence of ligament bands on one another. Variations could be generated in a similar manner as that described in the Methods, but they would be completed at the component level and at finer increments. Ultimately, these additional component variations would provide more training data for the neural networks, thereby strengthening

the predictions made by ANNs and subsequently offering more details about the role of soft tissues in the foot/ankle.

4.9 Overall Discussion and Future Directions

The objectives of this research were to (1) predict honed in stiffnesses for both patient-specific pre-operative and post-operative models for a single patient and (2) improve the predictive ability of these models. Feedforward and radial basis function networks were trained in both the pre- and post-operative cases, and of the networks tested, one optimal network of each type was selected. Performance measures, as demonstrated by mean square error and correlation, demonstrated good network performance and facilitated network choice. These networks were eventually used to predict ligament stiffnesses for the patient's pre- and post-operative X-ray data, which represented plausible computational kinematic scenarios, and the stiffnesses predicted did, in fact, result in improved predictive ability of the patient-specific foot/ankle models. Thus, it can be concluded that the objectives of this research were satisfied.

Furthermore, the work here provided some insight into the significance of specific ligament groupings on kinematic measures. Subsequent iterations of this research may investigate these ligament grouping/component – kinematic relationships such that knowledge of soft tissue properties and functionalities may expand in the future. This could be done by generating stiffness variations of ligament groupings at finer increments or by varying ligaments on a component-by-component basis such that the contributions of individual bands are better understood. These additional data pairs could then be supplied to the ANN for training in a similar manner as was noted in the current work. Generally,

the use of ANNs to optimize ligament stiffness inputs serves the purpose of developing a more representative computational foot/ankle model, and, in turn, this more representative model enhances the knowledge base regarding the foot/ankle and AAFD's effects on this joint complex. Additionally, the use of ANNs to improve a foot/ankle model suggests that ANNs could be applied to models of other physiologic systems, thereby making these other models more reflective of the respective systems, and patients, they are meant to represent. For example, insight into optimized values of particular ligaments for the patient model investigated in this work may be used to inform the ligament relationship with kinematics in other patient models within the AAFD cohort, and thus better characterize those models as well.

Alongside the investigation of ligament interplay, another expansion of the current research may include the study of additional machine learning techniques. Because the use of ANNs proved to be successful in optimizing ligament stiffness values, other methods such as support vector regression (SVR) or simulated annealing (SA) may be used for input optimization as well. Like ANNs, SVR also utilizes a cost function in determining a solution to a given problem; however, the technique looks for the maximum allowable error by determining a margin of acceptable error (dictated by a threshold value and support vectors, or input data that lie at the edges of the margin). Data that falls within this margin do not affect the function approximation, while tolerance of data falling outside of the margins is determined by a slack term [71]. As for SA, it, too, looks to minimize a cost function, but in order to avoid getting stuck in local minima, it allows for "hill climbing." In other words, SA will accept a solution in the near term that increases the value of the

cost function to ensure that a previously accepted "minimum" solution is, in fact, the global minimum. This method was utilized by Ewing et al. to predict soft tissue properties for a total knee arthroplasty [72], and thus could be applied to predict ligament properties for the foot/ankle. Ultimately, both SVR and SA could be used in the investigation of ligament properties and these methods' performance could then be compared to ANN performance.

Finally, the broadest impacts of this work may be seen in the future where a clinician may use improved patient-specific models to investigate various corrective procedures to relieve a particular ailment. With well-defined model inputs, attention would be focused solely on the impact of a given procedure on joint functionality. As a result, a well-characterized patient model would allow the clinician to quickly investigate the effects of different surgical procedures, and ultimately, determine the procedure that provided the patient with the best outcome.

Literature Cited

Literature Cited

[1] Liacouras PC, Wayne JS. 2007. Computational modeling to predict function of joints: application to the lower leg with simulation of two cadaver studies. J Biomech Eng. 129: 811-817.

[2] Spratley EM, Matheis EA, Hayes CW, Adelaar RS, Wayne, JS. 2013. Validation of a population of patient-specific adult acquired flatfoot deformity models. J Orthop Res. 31: 1861-1868.

[3] Lu Y, Pulasani PR, Derakhshani R, Guess TM. 2013. Application of neural networks for the prediction of cartilage stress in a musculoskeletal system. Biomed Signal Process Control. 8: 475-482.

[4] Iaquinto JM, Wayne JS. 2011. Effects of surgical correction for the treatment of adult acquired flatfoot deformity: a computational investigation. J Orthop Res. 29: 1047-1054.

[5] Cheung JT, Zhang M, Leung AK, Fan YB. 2005. Three-dimensional finite element analysis of the foot during standing--a material sensitivity study. J Biomech. 38: 1045-1054.

[6] Anderson DD, Goldsworthy JK, Shivanna K, Grosland NM, Pedersen DR, Thomas TP, Tochigi Y, Marsh JL, Brown TD. 2006. Intra-articular contact stress distributions at the ankle throughout stance phase-patient-specific finite element analysis as a metric of degeneration propensity. Biomech Model Mechanobiol. 5: 82-89.

[7] Sowmianarayanan S, Chandrasekaran A, Kumar RK. 2008. Finite element analysis of a subtrochanteric fractured femur with dynamic hip screw, dynamic condylarr screw, and proximal femur nail implants--a comparative study. Proc Inst Mech Eng H. 222: 117-127.

[8] Spratley EM, Wayne JS. 2011. Computational model of the human elbow and forearm: application to complex varus instability. Ann Biomed Eng. 39: 1084-1091.

[9] Majors BJ, Wayne JS. 2011. Development and validation of a computational model for investigation of wrist biomechanics. Ann Biomed Eng. 39: 2807-2815.

[10] Elmore KA, Wayne JS. 2013. Soft tissue structures resisting anterior instability in a computational glenohumeral joint model. Comput Methods Biomech Biomed Engin. 16: 781-789.

[11] Spratley EM. 2013. Patient-specific modeling of Adult Acquired Flatfoot Deformity before and after surgery [dissertation]. Richmond (VA): Virginia Commonwealth University.

[12] Johnson BA, Fallat LM. 1997. Comparison of tension band wire and cancellous bone screw fixation for medial malleolar fractures. J Foot Ankle Surg. 36(4), pp. 284–289.

[13] Draves DJ. 1986. Anatomy of the lower extremity. Baltimore, MD: Williams & Wilkins.

[14] Castro MD. 2007. Insufficiency fractures after total ankle replacement. Tech Foot Angle Surg. 6(1), p. 15.

[15] Levangie P, Norkin C. 2001. Joint structure and function: a comprehensive analysis. F.A. Davis Company, Philadelphia.

[16] Logan BM, Singh D, Hutchings RT. 2004. McMinn's color atlas of foot and ankle anatomy. 3rd ed. Edinburgh: Mosby Elsevier.

[17] Sarrafian SK. 1993. Anatomy of the foot and ankle: descriptive, topographic, functional. 2nd ed. Philadelphia, PA: Lippincott.

[18] Milner CE, Soames RW. 1998. Anatomy of the collateral ligaments of the human ankle joint. Foot Ankle Int. 19: 757-760.

[19] Taniguchi A, Tanaka Y, Takakura Y, Kadono K, Maeda M, Yamamoto H. 2003. Anatomy of the spring ligament. J Bone Joint Surg Am. 85: 2174-2178.

[20] Deland JT. 2008. Adult-acquired flatfoot deformity. J Am Acad Orthop Surg. 16: 399-406.

[21] Deland JT. 2012. Spring ligament complex and flatfoot deformity: curse or blessing? Foot Ankle Int. 33: 239-243.

[22] Williams G, Widnall J, Evans P, Platt S. 2013. MRI features most often associated with surgically proven tears of the spring ligament complex. Skeletal Radiol. 42: 969-973.

[23] Vulcano E, Deland JT, Ellis SJ. 2013. Approach and treatment of the adult acquired flatfoot deformity. Curr Rev Musculoskelet Med. 6: 294-303.

[24] Deland JT, de Asla, RJ, Sung IH, Ernberg LA, Potter HG. 2005. Posterior tibial tendon insufficiency: which ligaments are involved? Foot Ankle Int. 26: 427-435.

[25] Younger AS, Sawatzky B, Dryden P. 2005. Radiographic assessment of adult flatfoot. Foot Ankle Int. 26: 820-825.

. [26] Arangio GA, Wasser T, Rogman A. 2006. Radiographic comparison of standing medial cuneiform arch height in adults with and without acquired flatfoot deformity. Foot Ankle Int. 27: 636-638.

[27] Spratley EM, Matheis EA, Hayes CW, Adelaar RS, Wayne JS. 2015. Effects of degrees of surgical correction for flatfoot deformity in patient-specific computational models. Ann Biomed Eng. 43: 1947-1956.

[28] Louie PK, Sangeorzan BJ, Fassbind MJ, Ledoux WR. 2014. Talonavicular joint coverage and bone morphology between different foot types. J Orthop Res. 32: 958-966.

[29] Conti MS, Ellis SJ, Chan JY, Do HT, Deland JT. 2015. Optimal position of the heel following reconstruction of the stage II adult-acquired flatfoot deformity. Foot Ankle Int. 36: 919-927.

[30] Chan JY, Williams BR, Nair P, Young E, Sofka C, Deland JT, Ellis SJ. 2013. The contribution of medializing calcaneal osteotomy on hindfoot alignment in the reconstruction of the stage II adult acquired flatfoot deformity. Foot Ankle Int. 34: 59-66.

[31] Myerson MS, Corrigan J. 1996. Treatment of posterior tibial tendon dysfunction with flexor digitorum longus tendon transfer and calcaneal osteotomy. Orthopedics. 19(5):383–388.

[32] Saltzman CL, Nawoczenski DA, Talbot KD. 1995. Measurement of the medial longitudinal arch. Arch Phys Med Rehabil. 76: 45-49.

[33] Coughlin MJ, Kaz A. 2009. Correlation of Harris mats, physical exam, pictures, and radiographic measurements in adult flatfoot deformity. Foot Ankle Int. 30: 604-612.

[34] Hassoun MH. 1995. Fundamentals of Artificial Neural Networks, Cambridge, MA: The MIT Press

[35] Agatonovic-Kustrin S, Beresford R. 2000. Basic concepts of artificial neural network (ANN) modeling and its application in pharmaceutical research. J Pharm Biomed Anal. 22: 717-727.

[36] Haykin S. 2009. Neural networks and learning machines. Upper Saddle River, NJ: Pearson Prentice Hall.

[37] Bas B, Ozgonenel O, Ozden B, Bekcioglu B, Bulut E, Kurt M. 2012. Use of artificial neural network in differentiation of subgroups of temporomandibular internal derangements: a preliminary study. J Oral Maxillofac Surg. 70: 51-59.

[38] Specht DF. 1991. A general regression neural network. IEEE Trans Neural Netw. 2: 568-576.

[39] Taghavifar H, Mardani A. 2014. Application of artificial neural networks for the prediction of traction performance parameters. Journal of the Saudi Society of Agricultural Sciences.13: 35-43.

[40] Mahfouf M. 2006. Intelligent systems modeling and decision support in bioengineering. Norwood, MA: Artech House, Inc.

[41] Galushkin AI. 2007. Neural networks theory. Springer Science & Business Media.

[42] Massie DD, Curtiss PS. 2001. Neural network fundamentals for scientists and engineers.

[43] Beale MH, Hagan MT, Demuth HB. 2013. Neural Network Toolbox™, user's guide R2013b. Natick, MA: The MathWorks, Inc.

[44] Wettschereck D, Dietterich T. 1992. Improving the performance of radial basis function networks by learning center locations. Advances in neural information processing systems 4. San Mateo, CA: Morgan Kaufmann.

[45] Basheer IA, Hajmeer M. 2000. Artificial neural networks: fundamentals, computing, design, and application. J Microbiol Methods. 43: 3-31.

[46] Lavrenko V. (2015, August 31). *Backpropagation: how it works.* [Video file]. Retrieved from https://www.youtube.com/watch?v=An5z8lR8asY.

[47] Lavrenko V. (2015, August 31). *Neural Networks II: Backpropagation in detail.* [Video file]. Retrieved from https://www.youtube.com/watch?v=dKu911Zveb0.

[48] Abu-Mostafa Y. (2012, May 29). *Lecture 16--Radial Basis Functions.* [Video file]. Retrieved from https://www.youtube.com/watch?v=O8CfrnOPtLc.

[49] Masters T. 2013. Assessing and improving prediction and classification. [place unknown]: Timothy Masters.

[50] Heath G. 2015, April 30. Tutorial on neural net crossvalidation design. [Online forum comment]. Message posted to https://www.mathworks.com/matlabcentral/newsreader/view_thread/340857

[51] Graupe D. 2013. Principles of artificial neural networks. 3rd ed. World Scientific.

[52] Ahmed FE. Artificial neural networks for diagnosis and survival prediction in colon cancer. Mol Cancer 4:29.

[53] Eskinazi I, Fregly BJ. 2013. Surrogate knee contact modeling using artificial neural networks. In: *Proceedings of the ASME 2013 Summer Bioengineering Conference*. Sunriver, Oregon: American Society of Mechanical Engineers.

[54] Rae SA, Wang WJ, Partridge D. 1999. Artificial neural networks: a potential role in osteoporosis. J R Soc Med 92: 119-122.

[55] Lippman R. 1987. An introduction to computing with neural networks. IEEE ASSP Mag 3: 4-22.

[56] Moustris KP, Nastos PT, Larissi LK, Paliatsos AG. 2012. Application of multiple linear regression models and artificial neural networks on the surface ozone forecast in the greater Athens Area, Greece. Adv Meterol. 2012: 1-8.

[57] Peck CC, Dhawan AP, Meyer CM. 1993. Genetic algorithm based input selection for a neural network function approximator with applications to SSME health monitoring. In: *IEEE International Conference on Neural Networks*. IEEE.

[58] Dreiseitl S, Ohno-Machado L. 2003. Logistic regression and artificial neural network classification models: a methodology review. J Biomed Inform. 35: 352-359.

[59] Aktepe A, Ersoz S, Luy M. 2012. Backpropagation neural network applications for a welding process control problem. In C. Jayne, S. Yue & L. S. Iliadis (eds.), *EANN* 2012. CCIS 311: 193-202. London, UK: Springer.

[60] Kaufman JJ, Chiabrera A, Hatem M, Hakim NZ, Figueiredo M, Nasser P, Lattuga S, Pilla AA, Siffert RS. 1990. A neural network approach for bone fracture healing assessment. IEEE Eng Med Biol Mag. 9:23-30.

[61] Tu JV. 1996. Advantages and disadvantages of using artificial neural networks versus logistic regression for predicting medical outcomes. J Clin Epidemiol. 11: 1225-1231.

[62] Kurtser P, Levi O, Gontar V. 2012. Detection and classification of ECG chaotic components using ANN trained by specially simulation data. In C. Jayne, S. Yue & L. S. Iliadis (eds.), *EANN* 2012. CCIS 311: 193-202. London, UK: Springer.

[63] Lin JT, Bhattacharyya D, Kecman V. 2003. Multiple regression and neural networks analyses in composites machining. Composites Science and Technology. 63: 539-548.

[64] Chande RD, Ortiz-Robinson N, Hobson Hargraves R, Wayne JS. 2015. Application of artificial neural networks to improve predictive ability of computational joint models. In: Transactions of the 2015 Annual Meeting of the Orthopaedic Research Society; 2015 Mar

[65] Heath G. 2015, May 20. Another neural network regression tutorial using fitnet. [Online forum comment]. Message posted to https://www.mathworks.com/matlabcentral/newsreader/view_thread/341113

[66] Heath G. 2013, January 16. NN validation and data partition. [Online forum comment]. Message posted to https://www.mathworks.com/matlabcentral/answers/58761-nn-validation-and-data-partition

[67] Kuzniar K, Chudyba L. 2012. Neural networks for the analysis of mine-induced vibrations transmission from ground to building foundation. In C. Jayne, S. Yue & L. S. Iliadis (eds.), *EANN* 2012. CCIS 311: 193-202. London, UK: Springer.

[68] Kecman V. 2001. Learning and soft computing, support vector machines, neural networks, and fuzzy logic models. Cambridge, MA: The MIT Press.

[69] Gholipour A, Arjmand N. 2016. Artificial neural networks to predict 3D spinal posture in reaching and lifting activities; applications in biomechanical models. J Biomech. 49: 2946-2952.

[70] Heath G. 2012, July 24. Neural networks – trainbr and MSE. [Online forum comment]. Message posted to http://www.mathworks.com/matlabcentral/newsreader/view_thread/322012

[71] Abu-Mostafa Y. (2012, May 18). *Lecture 14--Support Vector Machines.* [Video file]. Retrieved from https://www.youtube.com/watch?v=eHsErlPJWUU&index=15&list=PLvx5ei9aEEqKgDZ7oaQGSToFi-QER4v1M.

[72] Ewing JA, Kaufman MK, Hutter EE, Granger JF, Beal MD, Piazza SJ, Siston RA. 2016. Estimating patient-specific soft-tissue properties in a TKA knee. J Orthop Res. 34: 435-443.

VITA

Ruchi Dilip Chande was born on February 28, 1984 in Syracuse, New York. She grew up mostly in California, and eventually attended the University of California, Berkeley where she earned her Bachelor of Science in Mechanical Engineering in May 2006. Immediately after graduation, Ruchi worked for Medegen, Inc. (now BD Biosciences) and spent the next three years assisting with tooling validations and process improvement, as well as design and development. With the encouragement of those she met at Medegen, Ruchi ventured across the country to attend Virginia Commonwealth University to pursue graduate studies in Biomedical Engineering in July 2009. There, she was a contributing member of the Orthopaedic Research Laboratory as well as a Licensing Intern at VCU's Tech Transfer Office. During this time, she earned the Erin McGurk grant for musculoskeletal research from the Orthopaedic Research Laboratory Alumni Council, among other recognition at conferences. She earned her Master of Science in 2012 and chose to continue on to the PhD program within Biomedical Engineering.

In addition to working on her doctoral research, Ruchi taught and assisted with various classes including Biomechanics and Anatomy. She had the opportunity to present at various conferences, and was later awarded the Alex M. Clarke Award for Academic Excellence in 2015. At the close of her PhD, Ruchi plans to re-engage in industry and public outreach so as to advance the engineering field.